EPA-600/4-76-025
June 1976

Environmental Monitoring Series

CALCULATED ACTINIC FLUXES (290 - 700 nm) FOR AIR POLLUTION PHOTOCHEMISTRY APPLICATIONS

Environmental Sciences Research Laboratory
Office of Research and Development
U.S. Environmental Protection Agency
Research Triangle Park, North Carolina 27711

RESEARCH REPORTING SERIES

Research reports of the Office of Research and Development, U.S. Environmental Protection Agency, have been grouped into five series. These five broad categories were established to facilitate further development and application of environmental technology. Elimination of traditional grouping was consciously planned to foster technology transfer and a maximum interface in related fields. The five series are:

1. Environmental Health Effects Research
2. Environmental Protection Technology
3. Ecological Research
4. Environmental Monitoring
5. Socioeconomic Environmental Studies

This report has been assigned to the ENVIRONMENTAL MONITORING series. This series describes research conducted to develop new or improved methods and instrumentation for the identification and quantification of environmental pollutants at the lowest conceivably significant concentrations. It also includes studies to determine the ambient concentrations of pollutants in the environment and/or the variance of pollutants as a function of time or meteorological factors.

This document is available to the public through the National Technical Information Service, Springfield, Virginia 22161.

EPA-600/4-76-025
June 1976

CALCULATED ACTINIC FLUXES (290-700 nm) FOR AIR POLLUTION PHOTOCHEMISTRY APPLICATIONS

by

James T. Peterson
Meteorology and Assessment Division
Environmental Sciences Research Laboratory
Research Triangle Park, NC 27711

U.S. ENVIRONMENTAL PROTECTION AGENCY
OFFICE OF RESEARCH AND DEVELOPMENT
ENVIRONMENTAL SCIENCES RESEARCH LABORATORY
RESEARCH TRIANGLE PARK, NC 27711

DISCLAIMER

This report has been reviewed by the Environmental Sciences Research Laboratory, U.S. Environmental Protection Agency, and approved for publication. Mention of trade names or commercial products does not constitute endorsement or recommendation for use.

AUTHOR'S AFFILIATION

The author is on assignment with the U.S. Environmental Protection Agency from the National Oceanic and Atmospheric Administration, U.S. Department of Commerce.

ABSTRACT

Calculations are presented of the actinic (spherically integrated) solar flux from 290 to 700 nm at solar zenith angles between 0 and 86°. The calculated values are obtained by using a radiative transfer program developed by Dave that accounts for molecular scattering, ozone absorption, and aerosol scattering and absorption. Input data consists of aerosol size distribution, aerosol number and ozone concentrations as a function of height, aerosol index of refraction, and the following as a function of wavelength: ozone absorption coefficient, molecular scattering coefficient, solar constant, and surface reflectivity. The calculated actinic flux values are evaluated for their dependence on variations of surface reflectivity, aerosol amount, ozone amount and station elevation. The variation of the actinic flux with altitude above the surface is discussed with emphasis on the change through the lowest kilometer of the atmosphere. Finally, the flux values presented here are compared to those of Leighton (1961); the differences in the methodology and input data between the two studies are illustrated. These calculated actinic flux data are useful for estimating photodissociation rate constants for application to photochemical air pollution problems.

CONTENTS

LIST OF FIGURES

LIST OF TABLES

ACKNOWLEDGEMENTS

Dale Coventry adapted the Dave radiative routines to the EPA computer. Craig Meisner was responsible for much of the execution of the many computer runs and tabulations of the actinic flux data. Margaret Wilder typed the drafts and final version of the manuscript. Their assistance is very gratefully acknowledged.

SECTION I

INTRODUCTION

The sun is the driving force for atmospheric photochemical reactions. In a polluted urban atmosphere constituents are produced and destroyed by a complex process that involves tens of specific kinetic reactions. The chemical products of this process strongly depend on the reactions between incident solar radiation and NO_2 and the aldehyde group (Dodge and Hecht, 1975).

This report is intended to update and amplify the pioneering work of Leighton (1961) on the application of solar radiation to air pollution photochemistry. In his book he used a simple, yet effective, radiative transfer model to calculate the actinic flux at the earth's surface at various zenith angles over the ultraviolet and visible solar spectrum. Many of Leighton's computational results were first reported by Leighton and Perkins (1956). Thus, most of the methodologies and input data that were available to him are now 20 years old. In addition, his tabulations apply only to the atmospheric level at the earth's surface. He also did not attempt to describe the sensitivity of his calculated fluxes to input data variability. Today, the radiative fluxes can be calculated in more detail on high speed computers, and more accurate data are available for the solar constant, surface reflectivity, total ozone amount, and atmospheric aerosol optical properties.

Leighton's actinic flux values have previously been used to determine photodissociation rate constants of several species, especially NO_2, as

a function of time of day (zenith angle). Such rate constants have been used in mathematical diffusion modeling of photochemical pollution (Reynolds et al., 1973) and in computer simulations of mixtures of reactive chemical species to evaluate various mechanisms for photochemical smog formation (Demerjian et al., 1974). Since actinic flux refers to the radiative energy incident on a molecule, it is difficult to measure or estimate from customary radiometric measurements with a flat sensor that is horizontal or normal to the sun. Thus, many users of actinic flux data have relied on Leighton's tabulations.

A table of theoretical values of the solar energy available for photochemical reactions, as a function of wavelength and solar zenith angle, has been prepared for general application. Also included are descriptions of the computational techniques and various aspects of the input data. The vertical variation of the actinic flux is discussed along with an analysis of the dependence of the actinic flux on typical variations of surface reflectivity, station elevation, total ozone amount and aerosol concentrations.

The body of this report is comprised of three main sections. The first describes the radiative transfer model used to calculate the actinic fluxes. The second focuses on input data necessary for the computations: atmospheric constituents, solar constant, surface reflectivity, etc. The last section discusses the results of the calculations and includes descriptions of the actinic flux values.

SECTION II

DESCRIPTION OF THE RADIATIVE TRANSFER MODEL

The basic radiative transfer model used for all calculations described in this report was developed for NASA[1] by Dave (1972). It includes molecular scattering, ozone absorption and aerosol scattering and absorption. Subsequently, absorption by water vapor, oxygen and carbon dioxide were included. Readers interested in the computational details are referred to a description of the complete model by Braslau and Dave (1973a, b). The model atmosphere is assumed to be cloudless, plane-parallel, and non-homogeneous. A monochromatic unidirectional solar flux is incident at the top with the bottom bounded by an idealized Lambert ground. The atmosphere contains arbitrary vertical distributions of ozone and aerosol number density and is divided into a finite number of layers. At each level the attenuated direct solar flux and upward and downward diffuse components are calculated. The program can be used to compute radiative intensities, including the degree, direction and ellipticity of polarization, but only flux values are reported here.

Much of the program computer time is used to calculate the optical properties of the model aerosols. First, coefficients are computed for the Legendre series representing the normalized scattering phase function for a unit volume containing an aerosol with a known size distribution.

---

[1]The FORTRAN computer code is available from NASA Goddard Space Flight Center, Greenbelt, MD as program RADTMO, # S00080.

Next, the Legendre coefficients are used to calculate the Fourier coefficients of a series representing the normalized aerosol scattering phase function. The argument of this series is the difference between the azimuth angles of incident and scattered radiation. The basic equation of radiative transfer for a given atmospheric model is then divided into a set of mutually independent integro-differential equations that represent the transfer of the n-th Fourier component of the scattered radiative intensity. Finally, each of these equations is individually solved by using an iterative procedure through a finite number of atmospheric layers. Use of the Fourier series to represent the normalized scattering phase function permits integration over azimuth to be carried out analytically. Integration over zenith angle (θ) is done numerically with $\Delta\theta=2°$. The result is the computation of the intensity of the radiation scattered in all directions emerging at selected levels of a model atmosphere.

Atmospheric aerosols are assumed to be spherical, be homogeneous, have a known refractive index, and have a given size distribution. Their size distribution and refractive index are assumed to be independent of height. The total number of particles per unit volume, however, can be varied for each atmospheric layer. The ozone content of each layer can also be specified as well as the ozone absorption coefficient for the wavelength in question. Additional input includes the Rayleigh scattering normal optical thickness; its value above any level is a linear function of pressure. The model atmosphere can be divided into 16, 20, 32, 40, 80, or 160 layers of varying pressure thicknesses. Forty layers were

selected for these computations as a compromise between greater computational accuracy from more layers and less computer time from fewer layers. The thinnest pressure layer (0.58 mb) is at the top of the atmosphere. Layer pressure thickness increases downward to 53.3 mb (675 m) at about 4 km height and then decreases to 17.4 mb (150 m) for the lowest layer. The lowest level ("the earth's surface") is not at the earth-atmosphere interface, but rather is considered to be within the atmosphere a few meters above the surface.

One of the strengths of this radiative model is its accuracy. Braslau and Dave (1973a) stated that their calculations of spectrally integrated flux values were accurate within about $\pm$0.5%. In this study, the computational scheme, itself, will have a slightly greater error because the atmosphere was divided into 40 layers, whereas Braslau and Dave used 160. Thus, the uncertainty in the computed actinic flux values should be governed by the uncertainties in the model input data, such as the solar constant and aerosol characteristics, which can exceed several percent. A large error, however, can be expected for results for the largest zenith angle (86°) reported here. In this instance, the sun is very near the horizon with an optical air mass of 12.4. The direct solar beam is almost entirely attenuated before reaching the earth's surface so that the small actinic fluxes are largely composed of multiply scattered radiation. Thus, the 86° values should be used cautiously since small percentage errors in the atmospheric constituents lead to larger percentage errors in the calculated fluxes.

ACTINIC FLUX MODIFICATIONS

Most radiative flux calculations used in atmospheric science are referenced to a flat, horizontal surface. The computer program used by Dave was so designed. In photochemical applications, however, the flux on a spherical surface, i.e., the flux "seen" by an ensemble of atmospheric molecules without fixed orientations, is more appropriate. This spherical flux was termed the actinic flux by Leighton (1961) after the flux that would be measured by a chemical actinometer[2] with radiation incident from all directions. The term actinic formally refers to radiant energy capable of initiating photochemical reactions (usually synonomous with ultraviolet frequencies) (Huschke, 1959). In any event, actinic flux as defined by Leighton is now in general use by the photochemical community and will be followed here.

The difference between the actinic and horizontal fluxes is further described in the following example. Consider only the radiation from one hemisphere, e.g., the downward-directed stream. Given the monochromatic, directionally-dependent radiative intensity $I_\lambda(\theta,\phi)$ at wavelength λ, where ϕ is the azimuth angle, the horizontal flux (F_λ) is defined by

---

[2]Leighton (1961, p.30) states that the actinic flux J_λ "is the irradiance which would be measured by a weakly absorbing chemical actinometer with a flat horizontal surface exposed to sun and sky." Since the actinic flux is the flux on a spherical surface, J_λ actually refers to the irradiance which would be measured by a spherical chemical actinometer exposed to incident radiation from all directions. Such devices have recently been constructed for NO_2 photodissociation by Jackson et al. (1975) and Sickles and Jeffries (1975).

$$F_\lambda = -\int_0^{2\pi}\int_0^{\pi/2} I_\lambda \cos\theta \sin\theta d\theta d\phi. \qquad (1)$$

The actinic flux, J_λ, for one hemisphere is defined by

$$J_\lambda = -\int_0^{2\pi}\int_0^{\pi/2} I_\lambda \sin\theta d\theta d\phi. \qquad (2)$$

These definitions for F_λ and J_λ differ only by the cos θ weighting factor. If the intensity is isotropic,

$$F_\lambda = 2\pi I_\lambda \int_0^{\pi/2} \cos\theta \sin\theta d\theta = \pi I_\lambda, \qquad (3)$$

and J_λ equals $2\pi I_\lambda$. Applying these definitions the Dave program was modified to compute the upward-directed and downward-directed components of the actinic flux at each level of the model atmosphere. Henceforth, unless otherwise noted, actinic flux will refer to the sum of its upward and downward components, i.e., the spherical flux obtained by integrating a form of (2) over both hemispheres.

Within the model the ground is assumed to be an idealized Lambert surface whereby the incident radiation is reflected with isotropic intensity. The reflectivity of the ground is defined as the ratio of the upward horizontal flux to the total (direct plus diffuse components) downward horizontal flux incident at the ground. Thus, for a given reflectivity, near the surface the upward actinic flux will be twice the upward horizontal flux since the upward stream is isotropic. If the downward intensity is isotropic, the reflectivities calculated from the actinic and horizontal fluxes will

be identical. At the other extreme, if the downward radiative stream consists only of the direct solar beam with the sun at the zenith, the actinic reflectivity will be twice the horizontal reflectivity, since the downward actinic and horizontal fluxes will be equal.

SECTION III

INPUT DATA

Several internal and boundary parameters must be specified to calculate the actinic flux. Properties of the atmospheric constituents--aerosols and ozone--were selected to represent general conditions in the continental U.S., but with some emphasis on typical urban concentrations. Emphasis was also given to the particular characteristics of the Los Angeles atmosphere since much practical and theoretical research has been done on its photochemical pollution. The number of spectral intervals and solar zenith angles chosen directly affected the amount of computer time. The solar constant and surface albedo values determined the upper and lower model boundary conditions.

DIVISION OF SOLAR SPECTRUM

The solution to the radiative transfer equation is strictly applicable only to monochromatic radiation. If the absorption or scattering coefficients of the atmospheric constituents change only gradually with wavelength and by a small amount, a single computation can be applied to a wavelength interval. Thus, to achieve the greatest computational accuracy the solar spectrum should be divided into many small intervals. This objective, however, was tempered because computer time had to be minimized by performing the computations over as few intervals as possible. The spectrum was divided arbitrarily into 48 intervals from 290 to 700 nm. Practically no solar energy at wavelengths less than 290 nm reaches the ground. Essentially all photochemical reactions applicable to urban air pollution problems occur at wavelengths less than 700 nm. Moreover, at longer wavelengths absorption of radiation by water vapor, a highly variable atmospheric consti-

tuent, becomes important. The spectral intervals are 5 nm wide between 290 and 420 nm, 10 nm wide between 420 and 580 nm, and 20 nm wide between 580 and 700 nm. The greatest resolution is at the shortest wavelengths where the ozone absorption changes rapidly and most photochemical reactions of interest occur.

OZONE

The general shape of the vertical ozone concentration profile used was that of McClatchey et al. (1972) for mid-latitude, summer conditions. All of their concentration values were multiplied by 0.893 to yield 0.285 cm-atm of total ozone in a vertical atmospheric column. Based on total ozone climatology (Craig, 1965; Komyhr et al., 1973), this is a representative, average value for the latitude of Los Angeles during summer and autumn. To account for an urban atmosphere, the ozone concentrations at the surface and 1 km levels of the model atmosphere were increased by a factor of 3.3 to 2×10^{-4} g m^{-3} (0.1 ppm). With this low-level increase, the total ozone in a vertical column was 0.295 cm-atm. The final ozone concentrations as a function of height are shown in Figure 1 and Appendix A. Data on ozone absorption coefficients were taken from Howard et al. (1960). The individual coefficients were plotted on semi-log paper versus wavelength and subjectively averaged over each spectral interval of the model. The values thus determined for the absorption coefficients for each interval are given in Appendix B. The wavelength-dependent total ozone normal optical thicknesses are also shown in Appendix B and Figure 2.

The ozone absorption coefficients used here are similar to those used by Leighton. The total ozone (0.295 cm-atm) used here, however, is significantly greater than the 0.22 cm-atm assumed by Leighton. The difference

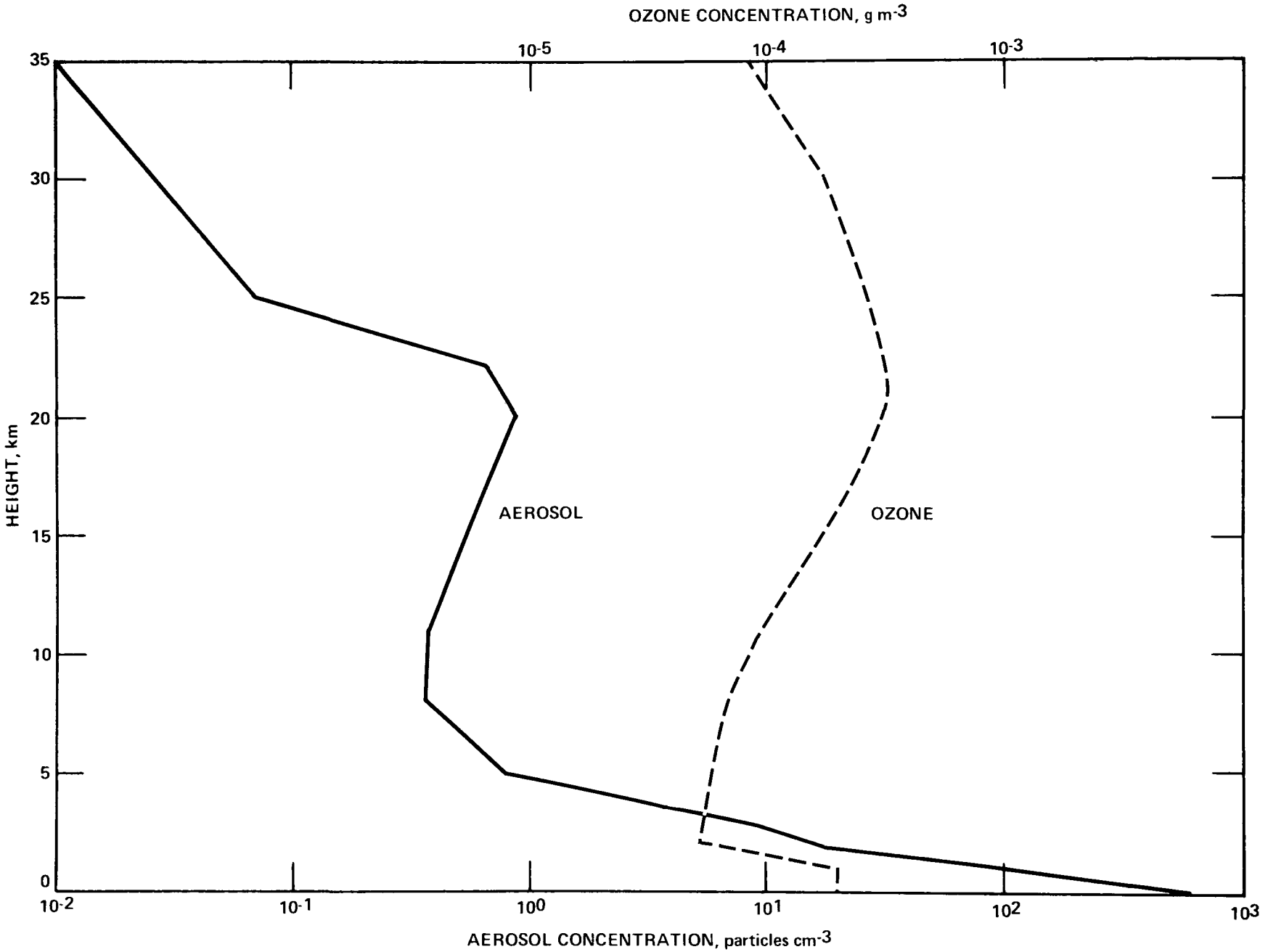

Figure 1. Variation with height (km) of aerosol number concentration (cm^{-3}) and ozone concentration ($g\ m^{-3}$) used as input for the actinic flux concentrations.

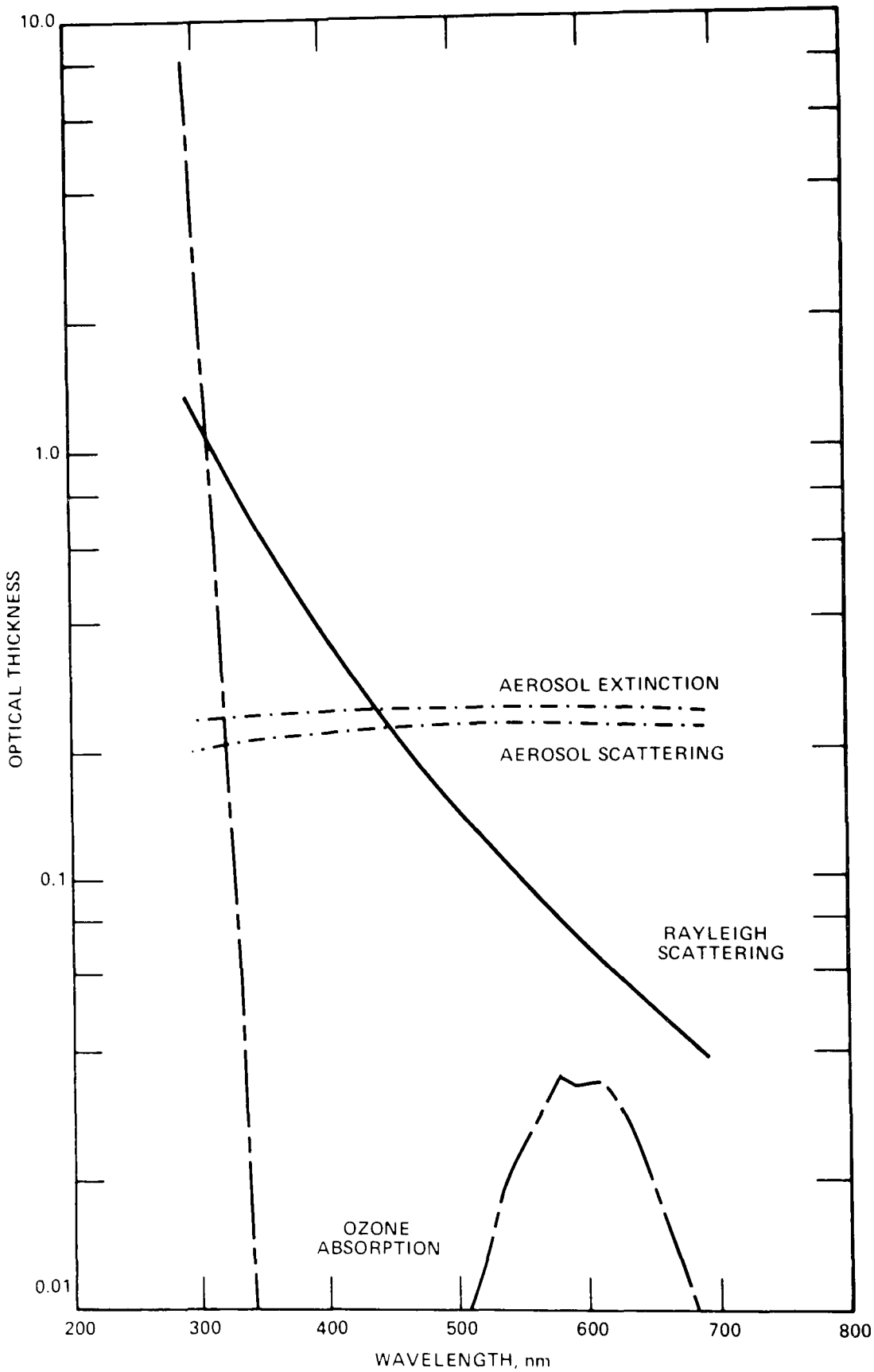

Figure 2. Normal optical thickness as a function of wavelength (nm) for aerosol scattering and extinction, Rayleigh scattering, and ozone absorption used as input for the actinic flux calculations.

in total ozone between the two works mainly results from the 1957 change in analysis procedure for ozone measurements by Dobson spectrophotometers. Craig (1961) suggests that all ozone concentrations reported before 1957 be increased by 35%. The larger ozone concentrations used here tend to reduce the calculated actinic fluxes relative to those calculated by Leighton.

AEROSOLS

An average representation of atmospheric aerosols is difficult to establish because of the day-to-day and place-to-place variation of many characteristics of aerosols. Thus, whenever the actinic flux data generated here are applied to a specific atmospheric situation the aerosol properties projected for the model will likely differ from those of that situation. Nonetheless, the characteristics of the aerosol model were defined so that they reasonably agree with various ambient measurements.

The Dave radiative model uses a single aerosol size distribution for all heights in the atmosphere. Following Braslau and Dave (1973a), the modified gamma distribution of Diermendjian (1969) for haze L conditions was selected to represent the aerosol distribution. The number of particles n ($cm^{-3}\mu m^{-1}$), of size r (μm), is given by

$$n(r) = ar^2 \exp(-br^{0.5}), \qquad (4)$$

where b = 15.12 and a determines the absolute number concentration. This distribution is a maximum for particles of 0.07 μm radius. For purposes of calculating the radiative characteristics of the aerosols, (4) was integrated between radii of 0.01 and 2.0 μm in increments of the size parameter ($2\pi r/\lambda$) of 0.2.

The vertical distribution of particle number density applied here was similar to the "average" height distribution model of Braslau and

Dave (1973a), except that concentrations at the surface and 1 km were increased by factors of 4 and 2, respectively (Figure 1 and Appendix A). This distribution, therefore, is more representative of urban conditions than that of Braslau and Dave. Combining these aerosol size and height distributions results in 4.99×10^7 total particles in a cm^2 atmospheric column.

The aerosols were assumed to be partly absorbing with an index of refraction (m), independent of height and wavelength, of m = 1.5 - 0.01i. Although this value is somewhat uncertain, especially in the imaginary part, it is in accord with recently measured values (Yamamoto and Tanaka, 1972).

Using these aerosol characteristics, the radiative properties of the aerosol ensemble were calculated as a function of height for the midpoint of each wavelength interval of the model. The aerosol normal optical thicknesses for scattering and scattering plus absorption (extinction) as a function of wavelength are presented in Appendix B and Figure 2. At 500 nm wavelength the extinction normal optical thickness has a value of 0.254, of which 91% is due to scattering. Its variation over the spectral region of interest is less than 7%. This can be compared to the value of 0.1 adopted by Rasool and Schneider (1971) for average global atmospheric dust content and the value of 0.23 measured by Herman et al. (1971) for typical haze conditions at the UCLA campus of Los Angeles, which is considerably west of the haziest sections of the Los Angeles area. The aerosol normal optical thickness of 0.254 from this study corresponds to a decadic turbidity of 0.11, which is similar to the annual average non-urban conditions over the eastern U.S., but slightly less than average annual values at U.S. urban stations

(Flowers et al., 1969).

Leighton used a much simpler approach to atmospheric aerosols. His aerosol extinction was assumed to be totally due to scattering. The scattered energy was assumed to be isotropic, with half the radiation propagating forward and half backward. His aerosol normal optical thickness showed more dependence on wavelength, varying between 0.390 and 0.140 at wavelengths of 300 and 700 nm, respectively. At 500 nm his value was 0.204, slightly less than that used here. Thus, his normal optical thickness for aerosols was greater over the ultraviolet region and less at longer wavelengths.

RAYLEIGH SCATTERING

Values of the molecular (Rayleigh) scattering normal optical thickness for standard sea level pressure were determined for the midpoint of each model wavelength interval from the data of Penndorf (1957). These values are presented in Figure 2 and Appendix B, where the -4 power wavelength dependence is evident. Values of atmospheric pressure with height are listed in Appendix A.

SURFACE ALBEDO

Since the actinic flux is sensitive to radiation propagating in all directions, the surface albedo (reflectivity) is a critical input parameter (Luther and Gelinas, 1976). Most natural and man-made materials have low albedos in the ultraviolet region with progressively larger values at longer wavelengths. The best estimate numbers used here, determined primarily from the experimental data of Coulson and Reynolds (1971), are: 290 to 400 nm (5%), 400 to 450 nm (6%), 450 to 500 nm (8%), 500 to 550 nm (10%), 550 to 600 nm (11%), 600 to 640 nm (12%), 640 to 660 nm (13.5%), and

660 to 700 nm (15%). As is customary, their data were derived from measurements of incident and reflected horizontal fluxes. As pointed out above, however, for a given albedo, the near-surface upward directed actinic flux is twice the horizontal flux because the reflected radiation is assumed isotropic.

The treatment of surface albedo in this report is different from that of Leighton. His calculations did not include the upward component of the actinic flux and thus, in effect, he assumed an albedo of zero. In a later section the sensitivity of these calculations will be discussed to show that a change of albedo from 0 to 10% results in increased actinic fluxes at the surface of about 10 to 20%, depending on wavelength and solar zenith angle.

SOLAR CONSTANT

Unfortunately, the wavelength dependent values of the solar constant, especially over the ultraviolet wavelengths, are still uncertain today. Values of the intensity of the extraterrestrial solar beam at the mean earth-sun distance reported by five sources as well as that used by Leighton are shown in Table 1. The earliest data by Johnson (Howard et al., 1960) are 7% to 11% higher in the ultraviolet region than the more recent measurements of Thekaekara (1974), DeLuisi (1975), and Arvesen et al., (1969). In contrast, Labs and Neckel (1968) list values in the ultraviolet significantly lower than the other sources. Even though the three most recent sources are in general agreement when summed over the ultraviolet, they disagree by up to 10% at specific wavelengths. For this report, the data of DeLuisi were used from 300 to 400 nm and those of Thekaekara elsewhere. DeLuisi's published monochromatic data were integrated trapezoidally to yield the values in Table 1 over 5 nm intervals. Any user of the actinic fluxes

TABLE 1. EXTRATERRESTRIAL SOLAR FLUX ($W\ m^{-2}$) WITHIN SPECIFIED WAVELENGTH INTERVALS (nm) USED BY LEIGHTON AND REPORTED BY FIVE SOURCES (SEE TEXT). VALUES FOR LEIGHTON AND LABS AND NECKEL FROM 290 THROUGH 420 nm ARE FOR 10 nm INTERVALS.

WAVELENGTH (nm)	LEIGHTON	JOHNSON	THEKAEKARA	DELUISI	ARVENSEN ET AL.	LABS & NECKEL
290-295		3.08	2.67		2.64	
295-300	6.3	3.02	2.75		2.78	5.14
300-305		3.00	2.79	2.70	2.78	
305-310	6.7	3.50	3.23	3.17	3.06	5.47
310-315		3.90	3.63	3.90	3.61	
315-320	8.2	4.05	3.99	3.92	3.75	6.70
320-325		4.65	4.51	4.09	3.75	
325-330	10.2	5.50	5.09	5.28	5.14	8.33
330-335		5.60	5.35	5.19	5.28	
335-340	11.1	5.60	5.39	4.89	4.87	9.16
340-345		5.80	5.36	5.09	5.14	
345-350	11.7	5.82	5.41	4.94	4.87	9.10
350-355		5.90	5.44	5.47	5.42	
355-360	11.6	5.85	5.38	4.92	4.87	9.65
360-365		6.15	5.50	5.34	5.00	
365-370	12.9	6.35	5.78	6.43	6.39	10.69
370-375		6.62	5.85	5.70	5.14	
375-380	13.2	6.18	5.69	6.24	6.12	10.57
380-385		6.00	5.55	5.07	5.00	
385-390	11.5	5.63	5.49	5.48	5.56	9.60
390-395		5.73	5.72	5.55	5.42	
395-400	12.0	7.00	6.55	6.62	6.67	11.51
400-405		8.71	7.68		8.76	
405-410		9.48	8.49		8.90	16.56
410-415		9.60	8.81		9.45	
415-420		9.67	8.80		9.45	17.25
420-430		18.27	16.93		17.60	16.83
430-440		18.10	16.94		17.50	16.95
440-450		21.10	19.15		20.10	19.54
450-460		21.78	21.47		21.00	20.33
460-470		21.64	20.49		20.80	20.12
470-480		21.50	20.49		21.10	20.14
480-490		20.47	19.94		19.80	19.12
490-500		20.50	19.54		20.00	19.80
500-510		19.60	19.16		19.74	19.25
510-520		19.25	18.45		18.63	18.53
520-530		19.40	18.45		19.04	18.80
530-540		19.75	18.15		19.18	19.39
540-550		19.65	17.54		18.90	18.77
550-560		19.32	17.15		18.49	18.61
560-570		19.02	17.04		18.35	18.48
570-580		19.14	17.16		18.77	18.53
580-600		37.87	33.92		36.70	36.08
600-620		35.66	32.67		35.31	34.80
620-640		34.22	31.43		34.06	33.27
640-660		32.99	30.26		31.97	31.34
660-680		32.06	29.13		31.83	30.71
680-700		30.34	28.00		30.30	29.39
300-400	109.1	108.83	101.68	99.98	97.86	90.78
290-700		674.0	613.3		651.8	628.5
TOTAL		1396	1353		1390	1365

presented in this report who prefers other solar constant data may make a linear adjustment to the actinic fluxes for any spectral interval. The preferred values used here are listed in Appendix B in W m^{-2} (column 2) and 10^{14} photons cm^{-2} sec^{-1} (column 3) summed over the given wavelength interval.

The values used by Leighton (based on Johnson's data) for the extraterrestrial solar flux averaged 9% higher over the ultraviolet region than those used herein. This difference contributed directly to the difference between the two studies in the calculated actinic fluxes.

The solar constant data discussed above are representative for the mean earth-sun distance, which occurs in early April and October. During other times of the year the extraterrestrial solar flux changes by as much as $\pm$3.4% due to changes in the earth-sun distance (Table 2). Although this correction is small, all actinic flux data presented here should be multiplied by the values of Table 2 when they are applied to a specific situation at a given time of year.

TABLE 2. CORRECTION FACTORS FOR EXTRATERRESTRIAL SOLAR FLUX VALUES DEPENDING ON EARTH-SUN DISTANCE AT VARIOUS TIMES OF YEAR.

DATE	CORRECTION FACTOR	DATE	CORRECTION FACTOR
Jan 1	1.033	July 1	0.966
Jan 15	1.032	July 15	0.967
Feb 1	1.029	Aug 1	0.970
Feb 15	1.024	Aug 15	0.974
Mar 1	1.018	Sept 1	0.982
Mar 15	1.011	Sept 15	0.989
Apr 1	1.001	Oct 1	0.998
Apr 15	0.993	Oct 15	1.006
May 1	0.984	Nov 1	1.015
May 15	0.978	Nov 15	1.022
June 1	0.971	Dec 1	1.027
June 15	0.968	Dec 15	1.031

SOLAR ZENITH ANGLES

Actinic fluxes were calculated for solar zenith angles of 0, 10, 20, 30, 40, 50, 60, 70, 78, and 86°. The optical air mass, uncorrected and corrected for atmospheric refraction, for each zenith angle is given in Table 3. The normal optical thicknesses shown in Figure 2 and Appendix B should be multiplied by the corresponding air mass value to determine the optical thickness for any zenith angle. When the sun is near the horizon (zenith angle of 86°), the long path length through the atmosphere almost depletes the entire direct solar beam. When the sun is within 20° of the zenith the atmospheric path length changes relatively little. At 35° N latitude, for example, zenith angles of 86, 78, and 70° occur about 20 minutes, 1 hour, and 1 hour 40 minutes, respectively, after sunrise and before sunset during late summer and early autumn. A listing of solar zenith angles as a function of true solar time and month is presented in Appendix C for latitudes of 20, 30, 40, and 50°N.

TABLE 3. OPTICAL AIR MASS AT SEA LEVEL, UNCORRECTED AND CORRECTED FOR ATMOSPHERIC REFRACTION, FOR VARIOUS SOLAR ZENITH ANGLES.

Zenith Angle (°)	0	10	20	30	40	50	60	70	78	86
Optical Air Mass										
Uncorrected	1.00	1.02	1.06	1.15	1.31	1.56	2.00	2.92	4.81	14.3
Corrected	1.00	1.02	1.06	1.15	1.31	1.56	2.00	2.90	4.72	12.4

SECTION IV

RESULTS

Input to the radiative transfer equations consisted of distributions of aerosols and ozone for a cloud-free atmosphere, the extraterrestrial solar flux, and the pressure-height relation. With this input the equations were solved for each of the ten solar zenith angles, each of the 48 spectral intervals from 290 to 700 nm wavelength, and for surface albedos of 0.0, 0.1, and the best estimate values. The resulting actinic fluxes at the surface are shown in Tables 4 and 5 for best estimate and zero albedos, respectively, in units of photons cm^{-2} sec^{-1} within the specified wavelength interval. The second column gives the power of ten by which each value should be multiplied.

The data in both tables show a general increase of actinic flux with increasing wavelength and decreasing solar zenith angle. The marked increase from 290 to about 340 nm results from the strong inverse dependence of ozone absorption on wavelength over that interval. The gradual actinic flux increase with wavelength beyond 340 nm results from decreasing Rayleigh scattering, increasing surface albedo and increasing solar constant photon flux. The actinic flux values at any given wavelength show a strong non-linear decrease with increasing solar zenith angle. This is shown in Figure 3 where the actinic fluxes determined from best estimate albedos are plotted as a function of zenith angle for several selected wavelengths. The flux change with zenith angle is slight for small angles, but large when the sun is near the horizon, similar to the change of optical air mass with zenith angle. Thus, during the early morning and late afternoon hours the solar energy available for photochemical reactions changes far

TABLE 4. CALCULATED ACTINIC FLUX (photons cm^{-2} sec^{-1}) AT THE EARTH'S SURFACE, AS A FUNCTION OF WAVELENGTH AND ZENITH ANGLE, WITHIN SPECIFIED WAVELENGTH INTERVALS FOR BEST ESTIMATE SURFACE ALBEDOS. THE SECOND COLUMN (EXP) LISTS THE POWER OF TEN BY WHICH ALL ENTRIES SHOULD BE MULTIPLIED.

WAVELENGTH (nm)	EXP	ZENITH ANGLE (°) 0	10	20	30	40	50	60	70	78	86
290-295	14	0.001	0.001	-	-	-	-	-	-	-	-
295-300	14	0.041	0.038	0.030	0.019	0.009	0.003	-	-	-	-
300-305	14	0.398	0.381	0.331	0.255	0.167	0.084	0.027	0.004	0.001	-
305-310	14	1.41	1.37	1.25	1.05	0.800	0.513	0.244	0.064	0.011	0.002
310-315	14	3.14	3.10	2.91	2.58	2.13	1.56	0.922	0.357	0.090	0.009
315-320	14	4.35	4.31	4.10	3.74	3.21	2.52	1.67	0.793	0.264	0.030
320-325	14	5.48	5.41	5.19	4.80	4.23	3.43	2.43	1.29	0.502	0.073
325-330	14	7.89	7.79	7.51	7.01	6.27	5.21	3.83	2.17	0.928	0.167
330-335	14	8.35	8.25	7.98	7.50	6.76	5.72	4.30	2.54	1.15	0.241
335-340	14	8.24	8.16	7.91	7.46	6.78	5.79	4.43	2.69	1.25	0.282
340-345	14	8.89	8.80	8.54	8.09	7.38	6.36	4.93	3.04	1.44	0.333
345-350	14	8.87	8.79	8.54	8.11	7.43	6.44	5.04	3.15	1.51	0.352
350-355	14	10.05	9.96	9.70	9.22	8.48	7.39	5.83	3.69	1.77	0.414
355-360	14	9.26	9.18	8.94	8.52	7.86	6.88	5.47	3.50	1.69	0.391
360-365	14	10.25	10.16	9.91	9.46	8.76	7.71	6.17	3.99	1.94	0.444
365-370	15	1.26	1.25	1.22	1.17	1.08	0.958	0.772	0.505	0.247	0.055
370-375	15	1.14	1.13	1.10	1.06	0.983	0.873	0.708	0.467	0.230	0.051
375-380	15	1.27	1.26	1.23	1.18	1.10	0.983	0.802	0.535	0.265	0.058
380-385	15	1.05	1.04	1.02	0.980	0.917	0.820	0.673	0.453	0.226	0.049
385-390	15	1.15	1.15	1.12	1.08	1.01	0.909	0.750	0.510	0.257	0.054
390-395	15	1.19	1.18	1.16	1.11	1.05	0.943	0.783	0.537	0.273	0.057
395-400	15	1.44	1.43	1.40	1.35	1.28	1.15	0.962	0.666	0.341	0.070
400-405	15	1.73	1.72	1.69	1.63	1.53	1.39	1.16	0.809	0.418	0.085
405-410	15	1.94	1.93	1.90	1.83	1.73	1.57	1.32	0.926	0.482	0.097
410-415	15	2.05	2.04	2.00	1.93	1.83	1.66	1.41	0.993	0.522	0.104
415-420	15	2.08	2.07	2.03	1.96	1.86	1.70	1.44	1.03	0.543	0.107
420-430	15	4.08	4.06	3.99	3.87	3.67	3.36	2.87	2.07	1.11	0.216
430-440	15	4.20	4.18	4.11	3.99	3.80	3.49	3.01	2.19	1.20	0.229
440-450	15	4.87	4.85	4.77	4.64	4.43	4.09	3.54	2.61	1.45	0.272
450-460	15	5.55	5.51	5.43	5.27	5.03	4.64	4.02	2.99	1.67	0.312

TABLE 4. CONTINUED

WAVELENGTH (nm)	EXP	ZENITH ANGLE (°) 0	10	20	30	40	50	60	70	78	86
460-470	15	5.68	5.65	5.57	5.42	5.17	4.79	4.17	3.12	1.77	0.325
470-480	15	5.82	5.79	5.70	5.55	5.31	4.91	4.32	3.26	1.87	0.341
480-490	15	5.78	5.75	5.67	5.53	5.29	4.93	4.33	3.29	1.90	0.339
490-500	15	5.79	5.76	5.68	5.54	5.31	4.96	4.37	3.34	1.95	0.344
500-510	15	5.99	5.96	5.87	5.71	5.47	5.09	4.47	3.41	1.99	0.340
510-520	15	5.88	5.86	5.77	5.62	5.38	5.02	4.43	3.40	2.00	0.340
520-530	15	5.98	5.95	5.87	5.72	5.48	5.11	4.52	3.47	2.04	0.336
530-540	15	5.98	5.95	5.87	5.72	5.48	5.12	4.52	3.48	2.05	0.326
540-550	15	5.88	5.85	5.77	5.62	5.40	5.04	4.46	3.44	2.03	0.317
550-560	15	5.94	5.91	5.83	5.68	5.44	5.08	4.49	3.46	2.04	0.312
560-570	15	5.99	5.96	5.88	5.73	5.49	5.13	4.54	3.50	2.06	0.306
570-580	15	6.12	6.09	6.00	5.85	5.61	5.24	4.63	3.57	2.10	0.301
580-600	16	1.25	1.24	1.22	1.19	1.14	1.07	0.951	0.737	0.439	0.064
600-620	16	1.26	1.26	1.24	1.21	1.16	1.08	0.963	0.748	0.448	0.065
620-640	16	1.27	1.26	1.24	1.17	1.10	1.10	0.980	0.771	0.473	0.074
640-660	16	1.30	1.30	1.28	1.25	1.20	1.13	1.01	0.803	0.502	0.086
660-680	16	1.33	1.33	1.31	1.28	1.23	1.16	1.04	0.828	0.527	0.096
680-700	16	1.33	1.32	1.30	1.27	1.23	1.16	1.04	0.839	0.541	0.104

TABLE 5. CALCULATED ACTINIC FLUX (photons cm^{-2} sec^{-1}) AT THE EARTH'S SURFACE, AS A FUNCTION OF WAVELENGTH AND ZENITH ANGLE, WITHIN SPECIFIED WAVELENGTH INTERVALS FOR SURFACE ALBEDO OF ZERO. THE SECOND COLUMN (EXP) LISTS THE POWER OF TEN BY WHICH ALL ENTRIES SHOULD BE MULTIPLIED.

WAVELENGTH (nm)	EXP	ZENITH ANGLE (°) 0	10	20	30	40	50	60	70	78	86
290-295	14	0.001	0.001	-	-	-	-	-	-	-	-
295-300	14	0.037	0.035	0.027	0.017	0.008	0.003	-	-	-	-
300-305	14	0.362	0.347	0.302	0.234	0.154	0.078	0.025	0.004	0.001	-
306-310	14	1.28	1.24	1.14	0.965	0.737	0.476	0.227	0.060	0.010	0.001
310-315	14	2.85	2.81	2.65	2.36	1.96	1.44	0.858	0.332	0.083	0.008
315-320	14	3.94	3.91	3.73	3.42	2.96	2.33	1.56	0.739	0.245	0.027
320-325	14	4.96	4.90	4.71	4.38	3.88	3.18	2.26	1.20	0.466	0.067
325-330	14	7.14	7.06	6.82	6.40	5.76	4.83	3.57	2.02	0.864	0.155
330-335	14	7.54	7.47	7.25	6.84	6.22	5.30	4.01	2.38	1.07	0.221
335-340	14	7.45	7.38	7.18	6.81	6.23	5.37	4.14	2.52	1.17	0.262
340-345	14	8.03	7.97	7.76	7.38	6.79	5.90	4.60	2.85	1.34	0.310
345-350	14	8.02	7.95	7.75	7.40	6.84	5.98	4.71	2.97	1.41	0.327
350-355	14	9.08	9.01	8.80	8.42	7.80	6.86	5.45	3.47	1.66	0.385
355-360	14	8.36	8.30	8.12	7.78	7.23	6.39	5.12	3.30	1.59	0.364
360-365	14	9.25	9.19	9.00	8.64	8.06	7.16	5.78	3.77	1.83	0.413
365-370	15	1.14	1.13	1.11	1.07	0.997	0.890	0.724	0.477	0.233	0.052
370-375	15	1.03	1.02	1.00	0.965	0.906	0.811	0.664	0.442	0.217	0.048
375-380	15	1.15	1.14	1.12	1.07	1.02	0.914	0.753	0.506	0.251	0.054
380-385	15	0.948	0.942	0.926	0.895	0.845	0.763	0.633	0.429	0.214	0.045
385-390	15	1.04	1.04	1.02	0.987	0.933	0.846	0.705	0.484	0.244	0.051
390-395	15	1.07	1.07	1.05	1.02	0.965	0.878	0.737	0.510	0.259	0.053
395-400	15	1.30	1.29	1.28	1.24	1.18	1.07	0.905	0.632	0.324	0.066
400-405	15	1.54	1.53	1.51	1.46	1.39	1.28	1.08	0.761	0.394	0.079
405-410	15	1.72	1.71	1.69	1.64	1.57	1.44	1.23	0.872	0.455	0.090
410-415	15	1.82	1.81	1.78	1.74	1.66	1.53	1.31	0.937	0.493	0.097
415-420	15	1.84	1.83	1.81	1.77	1.69	1.56	1.34	0.968	0.514	0.100
420-430	15	3.62	3.60	3.56	3.48	3.34	3.09	2.68	1.95	1.05	0.201
430-440	15	3.72	3.71	3.67	3.59	3.45	3.22	2.80	2.07	1.13	0.214
440-450	15	4.32	4.30	4.26	4.18	4.03	3.77	3.31	2.47	1.38	0.255

TABLE 5. CONTINUED

WAVELENGTH (nm)	EXP	ZENITH ANGLE (°) 0	10	20	30	40	50	60	70	78	86
450-460	15	4.73	4.72	4.67	4.59	4.43	4.16	3.68	2.78	1.57	0.287
460-470	15	4.85	4.84	4.80	4.71	4.56	4.30	3.82	2.91	1.66	0.299
470-480	15	4.96	4.95	4.91	4.83	4.69	4.43	3.96	3.04	1.76	0.314
480-490	15	4.93	4.93	4.88	4.81	4.68	4.43	3.97	3.07	1.79	0.341
490-500	15	4.94	4.93	4.89	4.82	4.69	4.46	4.01	3.12	1.84	0.319
500-510	15	4.93	4.92	4.88	4.82	4.69	4.46	4.02	3.14	1.85	0.310
510-520	15	4.85	4.83	4.80	4.74	4.62	4.41	3.98	3.13	1.86	0.309
520-530	15	4.93	4.92	4.88	4.82	4.71	4.49	4.06	3.20	1.91	0.524
530-540	15	4.92	4.92	4.89	4.83	4.71	4.49	4.07	3.21	1.92	0.299
540-550	15	4.84	4.83	4.80	4.75	4.64	4.43	4.02	3.17	1.90	0.291
550-560	15	4.81	4.80	4.78	4.72	4.61	4.41	4.00	3.17	1.90	0.285
560-570	15	4.86	4.85	4.82	4.76	4.66	4.45	4.04	3.20	1.92	0.279
570-580	15	4.96	4.95	4.92	4.87	4.76	4.55	4.13	3.27	1.96	0.276
580-600	16	1.01	1.01	1.00	0.992	0.971	0.931	0.848	0.676	0.409	0.059
600-620	16	1.01	1.00	1.00	0.990	0.970	0.931	0.852	0.682	0.417	0.060
620-640	16	1.01	1.01	1.00	0.995	0.978	0.943	0.867	0.703	0.439	0.068
640-660	16	1.01	1.01	1.01	1.00	0.986	0.954	0.883	0.724	0.463	0.078
660-680	16	1.01	1.01	1.01	1.00	0.990	0.960	0.893	0.740	0.482	0.087
680-700	16	1.01	1.01	1.01	1.00	0.988	0.961	0.897	0.749	0.496	0.094

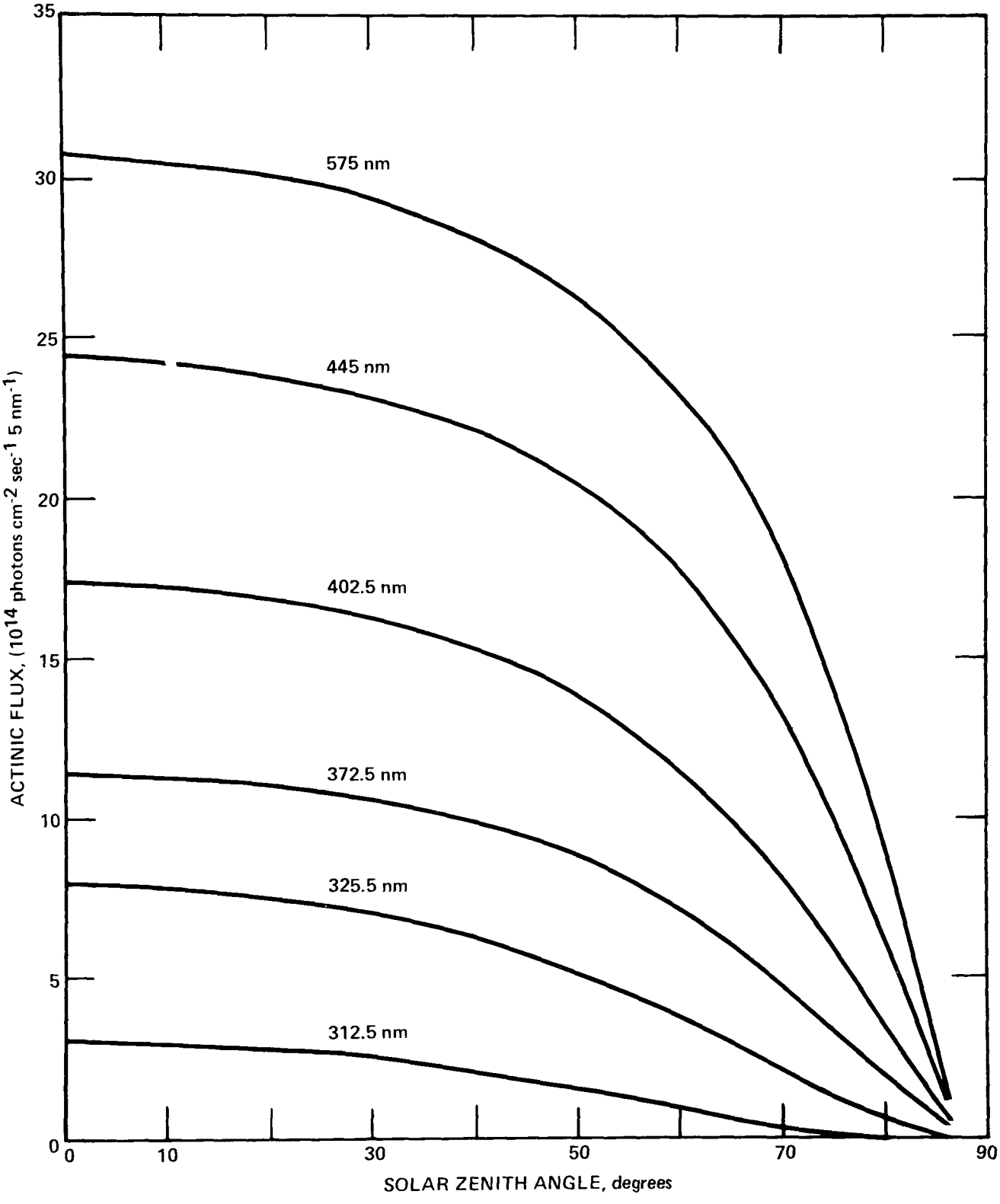

Figure 3. Calculated actinic flux (10^{14} photons cm^{-2} sec^{-1}) within five nm wavelength intervals, centered on the indicated wavelengths, at the earth's surface using best estimate albedos as a function of solar zenith angle(o).

more rapidly with time than during mid-day.

SENSITIVITY TESTS

The calculated actinic fluxes were evaluated for their dependence on variations of surface albedo, aerosol amount, ozone amount, and station elevation. The actinic flux values in Table 4 calculated from best estimate albedo data are intended for general use. However, the albedo of the earth's surface depends on type and amount of vegetation, type and moisture content of the soil, solar angle, urban or natural surface, snow cover, etc. (Lenschow et al., 1964). The dependence of the calculated actinic fluxes on surface albedo is shown in Table 6. The percentage increase of actinic flux for the lowest model level is presented, as a function of wavelength and solar zenith angle, corresponding to a change of surface albedo from zero to 10%. The greatest increases, exceeding 20%, generally occur at small zenith angles. A general trend is also evident toward smaller increases at larger zenith angles and longer wavelengths. The data in Table 6 can be used in conjunction with the actinic fluxes calculated for albedos of zero (Table 5) to determine the fluxes for other surface albedos when they are known to be different from the best estimate values. For albedos less than about 20%, the actinic fluxes are approximately linearly dependent on surface albedo.

The dependence of the actinic flux on atmospheric aerosol concentrations was studied next. The radiative model was rerun for best estimate albedos at four selected wavelengths (342.5, 402.5, 545, and 690 nm) for atmospheres with no aerosols and with aerosol concentrations twice those of the original values listed in Appendix A. The results for the lowest model level are shown in Table 7 as percentage changes in the calculated actinic fluxes

TABLE 6. PERCENTAGE INCREASE OF CALCULATED ACTINIC FLUX AT THE EARTH'S SURFACE, AS A FUNCTION OF SOLAR ZENITH ANGLE AND SELECTED WAVELENGTHS, RELATIVE TO THE VALUES IN TABLE 5 WHEN SURFACE ALBEDO IS INCREASED FROM 0.0 TO 10%.

WAVELENGTH (nm)	ZENITH ANGLE (°)									
	0	10	20	30	40	50	60	70	78	86
290-295	19.0	18.8	-	-	-	-	-	-	-	-
295-300	19.6	19.3	18.8	17.3	15.2	15.0	-	-	-	-
300-305	20.0	19.8	19.1	18.1	16.8	15.6	14.4	15.6	17.2	-
305-310	20.5	20.3	19.7	18.6	17.3	16.0	14.9	15.0	17.0	17.3
315-320	21.2	21.0	20.3	19.2	17.8	16.3	15.0	14.7	15.8	16.5
330-335	21.6	21.4	20.6	19.4	17.9	16.2	14.7	13.9	14.9	16.0
350-355	21.7	21.5	20.6	19.3	17.7	15.8	13.9	12.6	13.3	15.2
370-375	21.7	21.5	20.6	19.2	17.4	15.4	13.3	11.6	11.9	14.3
390-395	21.7	21.4	20.5	19.1	17.2	15.0	12.7	10.8	10.7	13.4
410-415	21.7	21.4	20.5	19.0	17.0	14.8	12.4	10.2	9.7	12.7
440-450	21.6	21.3	20.3	18.8	16.8	14.5	11.9	9.5	8.5	11.6
480-490	21.5	21.2	20.2	18.7	16.6	14.1	11.5	8.9	7.6	10.3
520-530	21.4	21.1	20.1	18.5	16.4	13.9	11.2	8.5	7.0	9.3
560-570	21.3	21.0	20.0	18.4	16.3	13.8	11.0	8.3	6.7	9.2
620-640	21.2	20.9	19.9	18.2	16.1	13.6	10.8	8.1	6.3	7.6
680-700	21.1	20.8	19.8	18.2	16.0	13.5	10.7	7.9	6.1	6.9

that would occur, relative to the values in Table 4, if the model aerosol concentrations were zero and double those used originally. The instance with no aerosols obviously represents the limit for clean atmospheres whereas the doubled concentrations occasionally could be exceeded over most large U.S. cities. Thus, the actinic fluxes for the no aerosol case are indicative of the maximum values that would occur at sea level for cloudless skies. At all wavelengths the changes increase as the solar zenith angle, and thus relative aerosol optical thickness, increases. Aside from the largest zenith angles, the percentage changes decrease with increasing wavelength although the aerosol optical thickness has little dependence on wavelength. At the longest wavelengths with the sun near the zenith, the actinic flux actually increases as the atmospheric aerosol concentration increases.

This results because the attenuation by Rayleigh scattering and ozone absorption is relatively small at these wavelengths, and near the surface multiple scattering by the aerosols causes some radiation to pass through a level of the atmosphere several times.

TABLE 7. PERCENTAGE CHANGE OF CALCULATED ACTINIC FLUX AT THE EARTH'S SURFACE USING BEST ESTIMATE ALBEDOS, AS A FUNCTION OF SOLAR ZENITH ANGLE AND SELECTED WAVELENGTHS, RELATIVE TO THE VALUES IN TABLE 4 WHEN MODEL AEROSOL CONCENTRATIONS ARE ZERO AND DOUBLED.

WAVELENGTH	ZENITH ANGLE (°)									
	0	10	20	30	40	50	60	70	78	86
340-345 nm										
NO AEROSOL	+8.2	+8.4	+8.8	+9.5	+10.7	+12.7	+16.1	+22.3	+26.5	+17.6
DOUBLE	-6.1	-6.3	-6.6	-7.3	-8.3	-10.1	-12.8	-16.1	-16.4	-12.5
400-405 nm										
NO AEROSOL	+5.8	+6.0	+6.4	+7.1	+8.3	+10.7	+15.3	+26.2	+46.8	+35.7
DOUBLE	-4.0	-4.1	-4.5	-5.3	-6.6	-8.8	-12.6	-19.4	-24.9	-15.9
540-550 nm										
NO AEROSOL	+0.9	+1.0	+1.2	+1.8	+2.9	+5.1	+10.4	+25.4	+67.1	+261.
DOUBLE	-0.8	-0.9	-1.4	-2.2	-3.7	-6.4	-11.6	-21.4	-33.6	-27.4
680-700 nm										
NO AEROSOL	-2.4	-2.4	-2.2	-1.8	-0.9	+1.1	+6.2	+21.7	+67.0	+447.
DOUBLE	+0.7	+0.6	+0.2	-0.6	-2.1	-4.9	-10.4	-20.8	-34.9	-35.5

Variations in the amount of total ozone in the atmosphere, most of which is in the stratosphere, can exceed 50% throughout the year from pole to equator (Craig, 1961). Within a season or latitude belt changes of total ozone of 10% are common. The effects of these changes on actinic flux at the earth's surface are confined to a narrow wavelength interval. At wavelengths greater than about 325 nm the ozone optical thickness is less than 10% of that for aerosols and Rayleigh extinction combined (see Figure 2). At wavelengths shorter than about 305 nm, the ozone optical thickness is so large that the absolute amount of energy reaching the

surface is small. Thus, outside of these limits only very large changes in total ozone will significantly influence the actinic flux. To estimate the effect of varying ozone levels, two additional model runs were undertaken at 302.5 and 322.5 nm wavelength using best estimate albedos. In each case the vertical ozone profiles were uniformly increased by 5%. The percentage decrease of actinic flux at the surface is shown in Table 8 for both wavelength intervals as a function of zenith angle. At the longer wavelength the change in ozone has a small effect, except when the sun is near the horizon. At 302.5 nm the actinic flux is sensitive to ozone variations; the change varied from near 10% to more than 21% for small to large zenith angles, respectively.

TABLE 8. PERCENTAGE DECREASE OF CALCULATED ACTINIC FLUX AT THE EARTH'S SURFACE USING BEST ESTIMATE ALBEDOS, AS A FUNCTION OF SOLAR ZENITH ANGLE AND SELECTED WAVELENGTHS, RELATIVE TO THE VALUES IN TABLE 4 WHEN MODEL OZONE CONCENTRATIONS ARE INCREASED BY FIVE PERCENT.

WAVELENGTH	ZENITH ANGLE (°)									
	0	10	20	30	40	50	60	70	78	86
300-305 nm	9.9	10.1	10.5	11.3	12.6	14.6	17.7	21.3	18.3	16.3
320-325 nm	1.7	1.7	1.8	1.9	2.2	2.5	3.1	4.3	6.3	10.5

All actinic flux calculations presented in this paper are based on a surface elevation of sea level. To test the sensitivity of the computations to higher station elevations a new set of fluxes was determined at four selected wavelengths for a surface elevation of 1500 m, or atmospheric pressure of 852 mb. For this test, using best estimate albedos, the vertical ozone and particle concentrations as a function of height above the surface were not changed from the original computations. Thus, the optical thicknesses for ozone absorption and Mie extinction were identical for both sets of

calculations. However, the Rayleigh scattering optical thickness at all wavelengths was reduced by a factor of 0.841 to account for the higher elevation.

The results of these calculations are shown in Table 9. The percentage increases of calculated actinic flux for the lowest model level for 1500 m surface elevation as compared to sea level elevation (Table 4), are presented as a function of wavelength and solar zenith angle. The tabulated values generally increase for shorter wavelengths and larger zenith angles. The effect of changing elevation on the calculated actinic fluxes generally is not large; the percentage increases are less than 5% except for the largest zenith angles.

TABLE 9. PERCENTAGE INCREASE OF CALCULATED ACTINIC FLUX AT THE EARTH'S SURFACE USING BEST ESTIMATE ALBEDOS, AS A FUNCTION OF SOLAR ZENITH ANGLE AND SELECTED WAVELENGTHS, RELATIVE TO THE VALUES OF TABLE 4 WHEN SURFACE ELEVATION IS INCREASED TO 1500 m.

WAVELENGTH	ZENITH ANGLE (°)									
	0	10	20	30	40	50	60	70	78	86
340-345 nm	2.1	2.3	2.6	3.2	4.2	5.7	8.1	11.4	12.4	7.5
400-405 nm	0.9	0.9	1.1	1.5	2.1	3.0	4.6	7.6	10.9	6.7
540-550 nm	0.2	0.2	0.2	0.4	0.5	0.9	1.4	2.4	4.3	4.7
680-700 nm	0.02	0.02	0.05	0.1	0.2	0.3	0.5	1.0	1.7	2.8

VARIATION OF ACTINIC FLUX WITH ALTITUDE

For application to urban photochemical problems, one of the most important aspects of these calculations is the variation of actinic flux with altitude above the surface, especially through the surface-based mixing height of the atmosphere. The data available on this subject to date have resulted mainly from occasional ultraviolet radiometric measurements of the horizontal flux over Los Angeles (Nader, 1965; Peterson

and Flowers, 1975). As will be shown below, the actinic flux typically shows a marked increase through the lowest few kilometers of the atmosphere. The more intense radiation aloft could partly explain the occurrence of higher ozone concentrations at the base of, or within, the subsidence temperature inversion over Los Angeles than at the surface as observed by Edinger (1973) and Gloria et al., (1974).

For the computations of this paper, the atmosphere was divided into 40 layers and the actinic fluxes were calculated by the radiative transfer model at each atmospheric level. Examples of the variation with height of the upward (F^+) and downward (F^-) components and total (F^T) actinic flux for solar zenith angles of 20°, 50°, and 78° are shown in Figures 4, 5, and 6 for wavelengths 332.5, 412.5, and 575 nm, respectively. The fluxes have all been normalized to a solar constant value of pi. Although the model output extended above 45 km, the height scale of the figures was abbreviated to 25 km, since only small changes occurred above that height.

At the surface, the upward component of the actinic flux depends on the direct and diffuse parts of the downward component and the surface albedo. Generally, the upward component increases rapidly with height near the earth's surface, but the rate of change with height decreases at progressively higher levels. Above 10 km or so, the greatest relative values of the upward flux occur at short wavelengths and small zenith angles. The downward component generally increases slightly from the top of the atmosphere down to about 10 to 15 km, except at the largest zenith angles, as atmospheric scattering redirects some of the upward stream back downwards. The greatest increases occur at short wavelengths

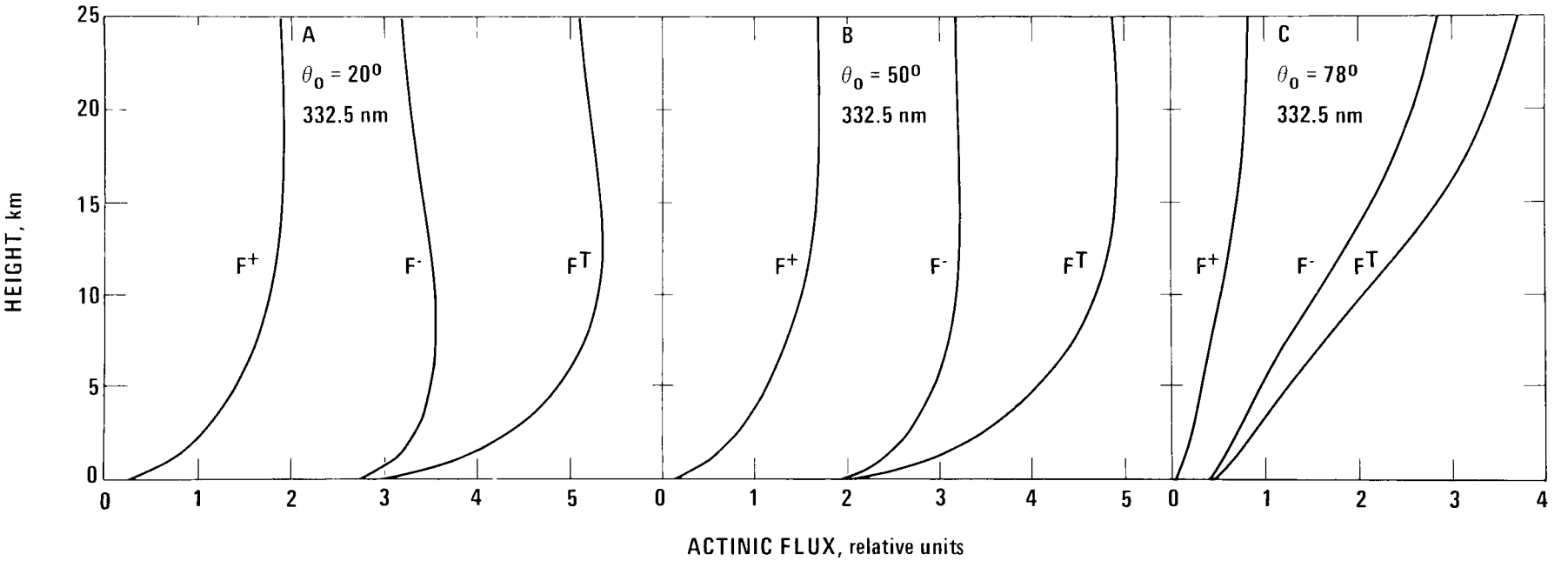

Figure 4. Calculated actinic flux (units relative to solar constant of pi) at the earth's surface using best estimate albedos for the upward-directed component (F^+), downward-directed component (F^-), and their sum (F^T) as a function of height at 332.5 nm wavelength for (a) solar zenith angle θ_0 of 20°, (b) 50°, and (c) 78°.

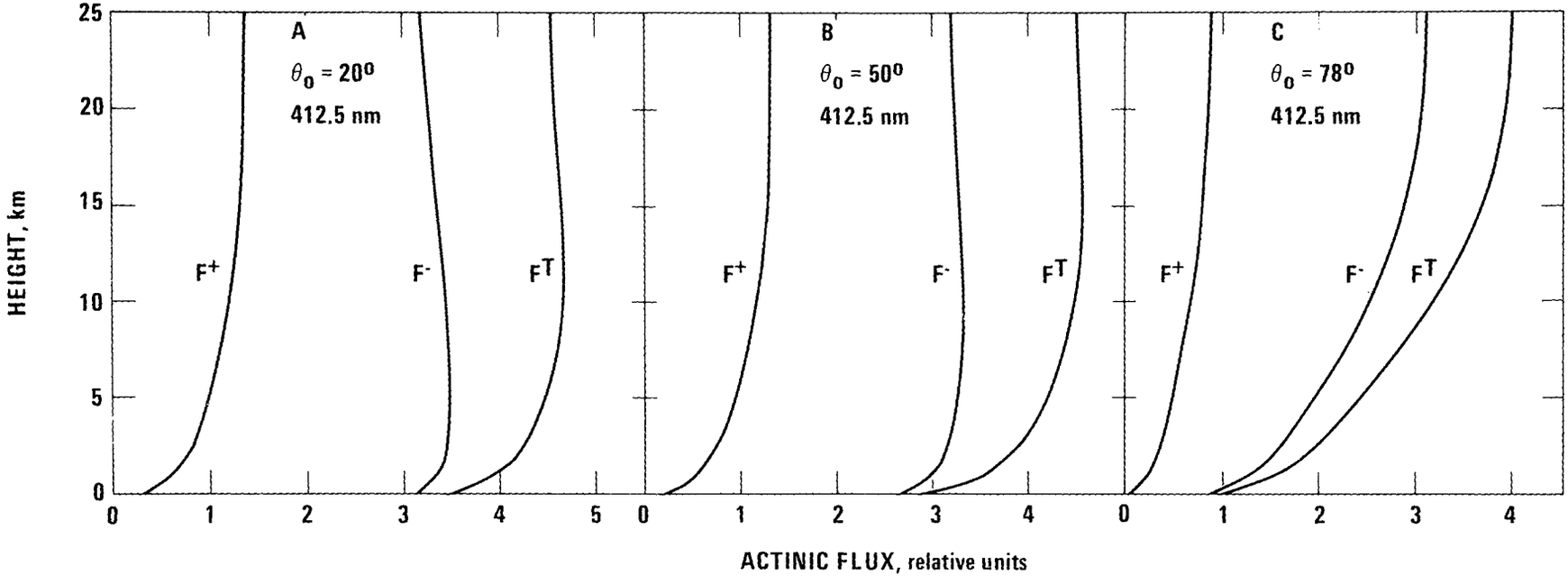

Figure 5. Calculated actinic flux (units relative to solar constant of pi) at the earth's surface using best estimate albedos for the upward-directed component (F^+), downward-directed component (F^-), and their sum (F^T) as a function of height at 412.5 nm wavelength for (a) solar zenith angle θ_0 of 20°, (b) 50°, and (c) 78°.

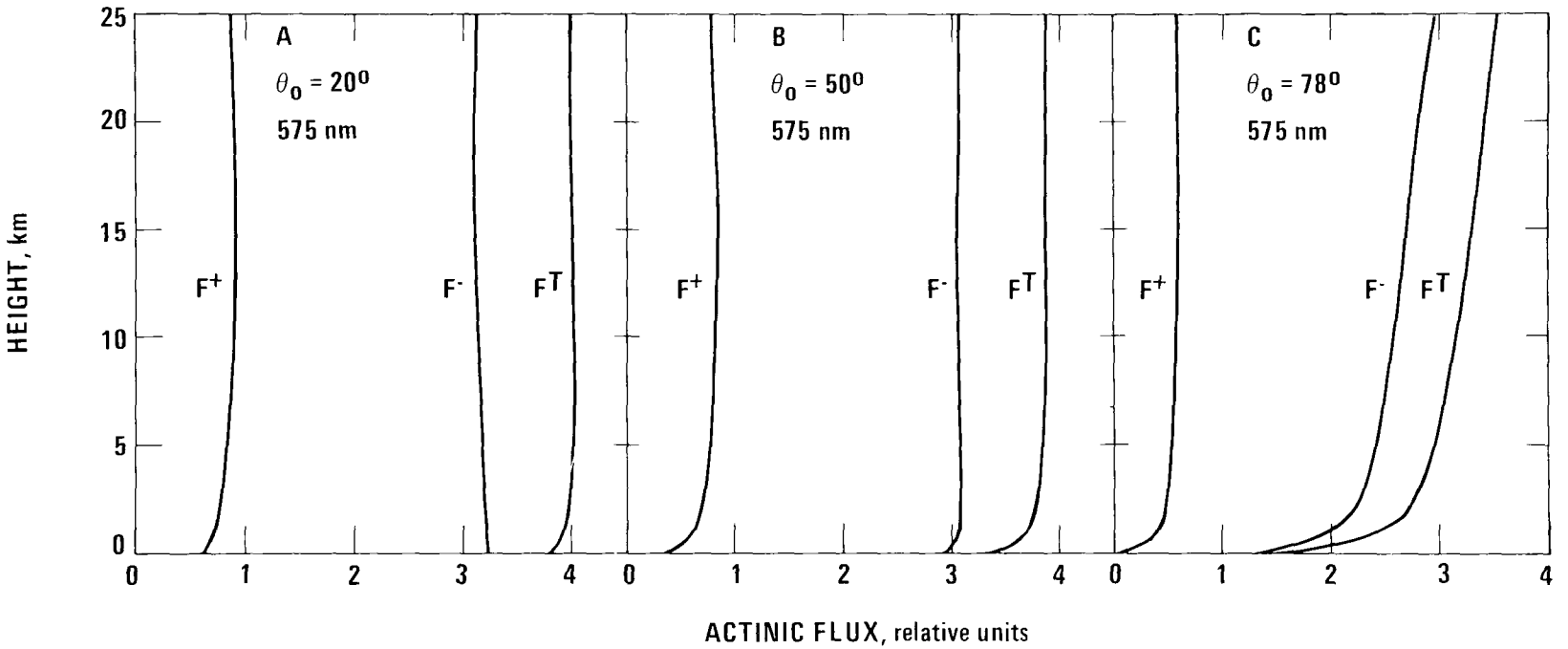

Figure 6. Calculated actinic flux (units relative to solar constant of pi) at the earth's surface using best estimate albedos for the upward-directed component (F^+), downward-directed component (F^-), and their sum (F^T) as a function of height at 575 nm wavelength for (a) solar zenith angle θ_0 of 20^o, (b) 50^o, and (c) 78^o.

and with a high sun. The downward component then decreases at progressively lower heights through the troposphere. The greatest rate of change occurs near the surface where high aerosol and ozone concentrations deplete the downward stream by absorption and back scattering.

Since both the upward and downward components change rapidly near the earth's surface, the total actinic flux also exhibits this change with height. In several cases shown in Figures 4 to 6, the total flux more than doubles between the surface and 5 km. The dependence of the vertical profiles of actinic flux on optical thickness is evident by comparing Figures 4c and 6a. In the former case, the combined vertical optical thickness for all atmospheric constituents is 1.066; the optical air mass is 4.81. The large atmospheric attenuation causes a substantial decrease of the downward stream. Since 74% of the optical thickness is due to Rayleigh scattering, much of the decrease occurs above the near-surface layer of high aerosol concentrations. At 10 km the actinic flux is already reduced to about one-half of its extraterrestrial value. In the latter case (575 nm, 20°), the vertical optical thickness is only 0.370 with an optical air mass of 1.06. With this relatively small atmospheric attenuation the actinic flux shows little change with height. Since atmospheric aerosols account for 69% of the optical thickness, the components of the actinic flux change most noticeably in the layer of high aerosol concentrations near the earth's surface.

The percent increase of the total actinic flux between the surface and 980 m (the fourth model level above the surface) was determined for each model run with best estimate albedos. These data are presented in Table 10 for selected wavelengths and all zenith angles. A strong

TABLE 10. PERCENTAGE INCREASE OF THE CALCULATED ACTINIC FLUX USING BEST ESTIMATE ALBEDOS, AS A FUNCTION OF SOLAR ZENITH ANGLE AND SELECTED WAVELENGTHS, AT 980 m ALTITUDE RELATIVE TO THE VALUES FOR THE EARTH'S SURFACE IN TABLE 4.

WAVELENGTH (nm)	ZENITH ANGLE (°)									
	0	10	20	30	40	50	60	70	78	86
290-295	63.7	64.7	-	-	-	-	-	-	-	-
295-300	48.9	49.6	51.8	55.6	61.3	68.9	-	-	-	-
300-305	41.4	41.9	43.6	46.4	50.8	56.8	63.9	63.0	51.4	-
305-310	37 5	37.9	39.3	41.7	45.4	50.6	57.5	61.9	52.8	47.5
315-320	34.5	34.2	35.3	37.3	40.5	45.1	51.6	58.9	56.6	46.9
325-330	30.2	30.6	31.7	33.6	36.6	41.0	47.5	56.2	57.5	45.7
335-340	27.6	28.0	29.1	31.0	33.9	38.3	45.0	55.1	59.7	45.1
345-350	25.3	25.7	26.8	28.7	31.6	36.0	43.0	54.4	62.3	44.8
355-360	23.3	23.7	24.8	26.6	29.5	34.1	41.3	53.7	65.1	45.2
365-370	21.5	21.9	22.9	24.7	27.7	32.1	39.6	52.9	68.0	46.2
375-380	19.8	20.2	21.3	23.1	26.0	30.5	38.1	52.3	70.6	48.2
385-390	18.4	18.8	19.8	21.6	24.4	29.0	36.7	51.6	73.1	51.1
395-400	17.1	17.4	18.4	20.2	23.0	27.5	35.4	50.9	75.4	55.4
405-410	15.3	15.6	16.6	18.3	21.1	25.7	33.6	49.6	76.4	60.0
415-420	14.2	14.5	15.5	17.2	20.0	24.5	32.5	48.9	78.1	67.1
430-440	12.5	12.9	13.8	15.5	18.3	22.7	30.8	47.9	80.5	82.4
450-460	9.8	10.1	11.1	12.7	15.4	19.9	28.1	45.7	81.3	102.
470-480	8.4	8.8	9.7	11.3	13.9	18.5	26.7	44.8	83.0	128.
490-500	7.3	7.6	8.5	10.1	12.7	17.2	25.5	44.1	84.3	154.
510-520	5.4	5.7	6.5	8.1	10.7	15.2	23.6	42.4	84.0	177.
530-540	4.5	4.8	5.7	7.2	9.8	14.2	22.6	41.8	84.8	201.
550-560	3.4	3.6	4.5	6.0	8.5	13.0	21.4	40.7	84.6	222.
570-580	2.7	3.0	3.8	5.2	7.8	12.2	20.7	40.2	85.0	242.
600-620	1.4	1.6	2.4	3.9	6.4	10.7	19.2	39.0	84.5	273.
640-660	0.0	0.3	1.0	2.4	4.9	9.2	17.7	37.3	83.1	300.
680-700	-1.0	-0.9	-0.1	1.2	3.6	7.9	16.3	35.9	81.6	318.

dependence can be seen between the vertical divergence of actinic flux and both wavelength and zenith angle. At wavelengths less than 330 nm, the change of actinic flux in the lowest kilometer of the atmosphere exceeds 30% at all solar angles. The change exceeds 50% over much of the spectrum for zenith angles of 70° and greater. In contrast, at long wavelengths in combination with a high sun the flux increase is less than 10%. Although the largest percentage changes of actinic flux occur at the largest zenith angles, the greatest absolute changes typically occur at smaller zenith angles. This results because at low sun angles the downward stream is strongly attenuated before it gets to the 1 km level.

An example of the practical importance of the vertical variation of actinic flux is its relation to the NO_2 photodissociation rate constant, a critical parameter in photochemical smog models. The NO_2 rate constant is computed by summing the product of the actinic flux, the NO_2 absorption coefficient, and the quantum yield from 290 to about 420 nm. A rough estimate of the difference in the rate constant through the lowest kilometer of the model atmosphere can thus be obtained from Table 10. These data suggest an NO_2 rate constant increase of about 25% for small zenith angles, about 35% at 50°, to more than 60% at 78°. Rate constant changes throughout (horizontally and vertically) the mixing layer of only 10% have been shown, by a contemporary photochemical diffusion model, to have a measureable change on surface ozone concentrations in the Los Angeles Basin (Peterson and Demerjian, 1976). Therefore, the vertical rate constant changes identified here likely will noticeably impact on calculated ozone concentrations. Actinic flux values, as a function of zenith angle and wavelength

(290 to 440 nm), for each of the lowest 11 model levels (surface to 4.21 km) have been tabulated by the author and can be supplied upon request.

COMPARISON TO LEIGHTON

This study was undertaken to update and improve the actinic flux calculations of Leighton. Besides the intracacies of the radiative model calculations, differences in four specific areas led to discrepancies between Leighton's results and those of this study. First and most important, Leighton effectively assumed a surface albedo of zero, whereas in this report the surface albedo varied between 5% and 15% as a function of wavelength. Consequently, due to the albedo differences alone, the actinic fluxes calculated here were some 5 to 11% higher in the UV and up to about 30% higher at the longest wavelengths (see Table 6) than those of Leighton. Second, recent measurements have indicated that the solar constant data available to Leighton were too high. The values herein were overall about 9% less than those used by Leighton. Third, in 1957 the scheme used to deduce total ozone amounts from Dobson spectrophotometer data was changed so that contemporary values are about 35% higher than the pre-1957 values. In the preceeding discussion on sensitivity tests, the actinic fluxes were shown to be dependent on changes of ozone concentrations over a narrow spectral region in the ultraviolet. Thus, the higher climatological values of total ozone used here caused significantly lower actinic fluxes at wavelengths less than about 325 nm. Fourth, the optical thickness for aerosols used by Leighton varied widely with wavelength whereas for this report it was fairly constant. The values for the two studies were similar at 420 nm with Leighton's data greater (smaller) at shorter (longer) wavelengths. His extinction was totally

due to scattering whereas for these computations some 8 to 15% of the extinction was due to absorption. The most important difference, however, was Leighton's assumption that half the scattered radiation was directed backward whereas for the aerosol ensemble used herein the large majority was directed forward. Thus, Leighton's aerosols, especially in the ultraviolet, caused more depletion of the actinic flux than did the aerosols used here.

Since Leighton's computations yielded actinic fluxes only at the surface, a comparison between the two studies must be restricted to that level. For the solar zenith angles common to both studies, the actinic fluxes (using best estimate albedos from this report) were summed over three spectral intervals: 295 to 395 nm, 395 to 450 nm, and 450 to 700 nm. These divisions were selected since within each interval the differences between the studies were similar. For each broad spectral interval and zenith angle the percentage difference between the results presented here in comparison to Leighton's data are shown in Table 11. Generally, the actinic flux values computed here are lower over the ultraviolet region, slightly higher within the middle interval, and considerably greater than Leighton's numbers throughout the longer wavelength region. Much

TABLE 11. PERCENTAGE DIFFERENCE BETWEEN THE CALCULATED ACTINIC FLUX VALUES AT THE EARTH'S SURFACE FROM THIS STUDY (USING BEST ESTIMATE ALBEDOS) AND THOSE OF LEIGHTON SUMMED OVER SELECTED WAVELENGTH INTERVALS FOR SELECTED SOLAR ZENITH ANGLES.

WAVELENGTH (nm)	ZENITH ANGLE (°)			
	0	20	40	60
295-395	-6.1	-6.4	-5.5	-4.3
395-450	+2.4	+2.1	+3.4	+5.9
450-700	+18.8	+18.4	+17.0	+15.7

of the dependence on wavelength of the differences between the two reports, stems from the differences in the treatment of surface albedo.

The absolute actinic fluxes for the two studies are shown graphically as a function of wavelength for zenith angles of 20° and 60° in Figures 7 and 8, respectively. The comparisons shown in Table 11 are again evident in the figures. The actinic fluxes generally increase with wavelength in response to changes of the solar constant photon flux, optical thickness, and surface albedo. All values for 60° zenith angle are less than the corresponding values at 20°, a result of the greater atmospheric attenuation as the optical air mass increases.

CLOUDS

Because of the importance of solar radiation, high photochemical pollutant concentrations usually occur when no, or few, clouds are present. Results from a numerical diffusion model for Los Angeles, for example, showed that when overcast stratus occurred oxidant concentrations were generally reduced to 10 to 20% of their expected values for clear skies (Peterson and Demerjian, 1976). However, the model results also suggested that even high altitude cirrus clouds could cause a measureable decrease in oxidant concentrations.

All actinic flux data presented in this report were calculated for cloudless sky conditions. If these data are to be applied during cloudy conditions, they can be modified by either of two approximate methods. The first method, suggested by Leighton, is based on measurements of total solar flux during clear and cloudy skies by Haurwitz (1948). He determined cloud transmissivities as a function of zenith angle for

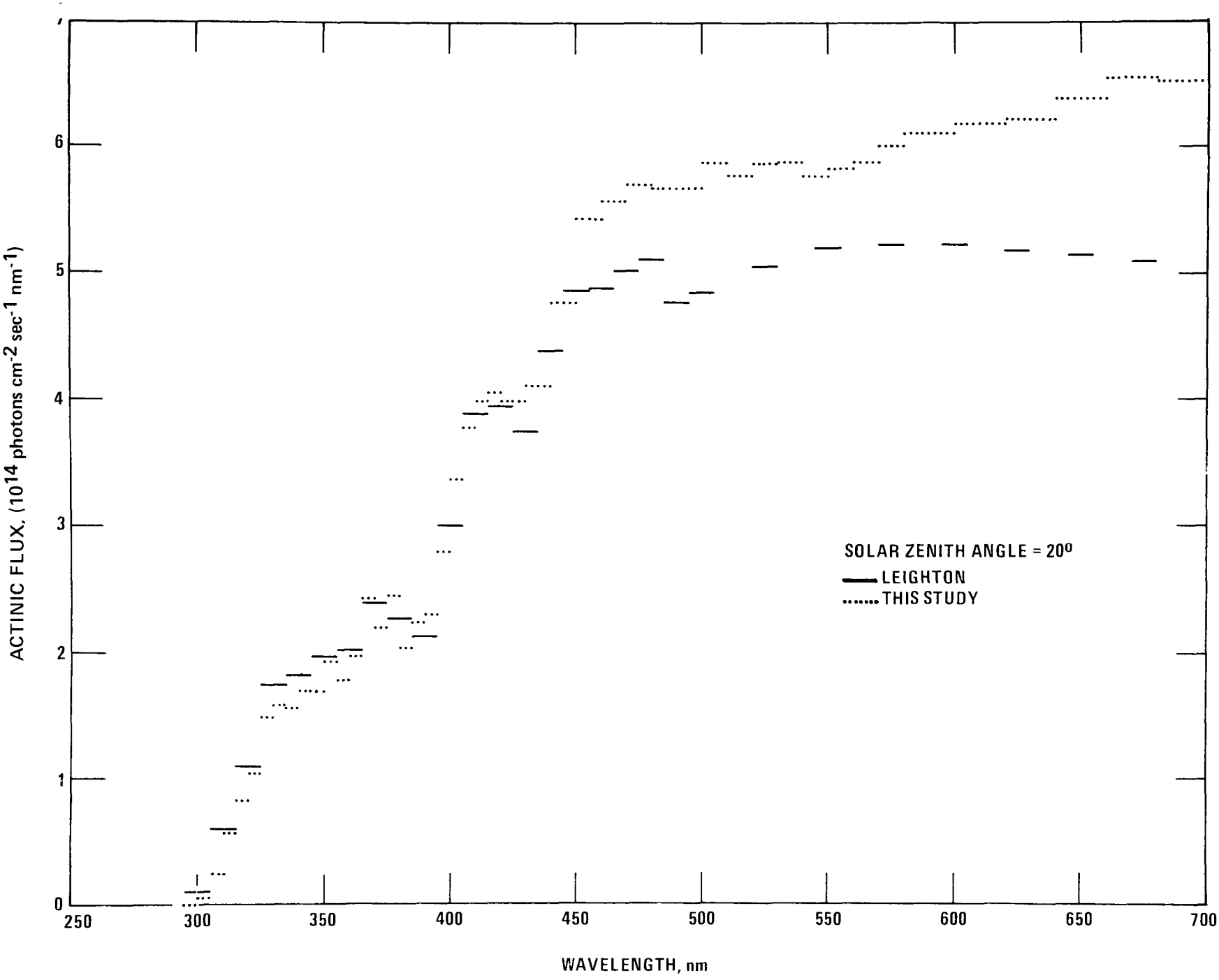

Figure 7. Calculated actinic flux (10^{14} photons cm^{-2} sec^{-1} nm^{-1}) averaged over indicated wavelength intervals (nm) at the earth's surface for solar zenith angle of 20° from this study (using best estimate albedos) and from Leighton.

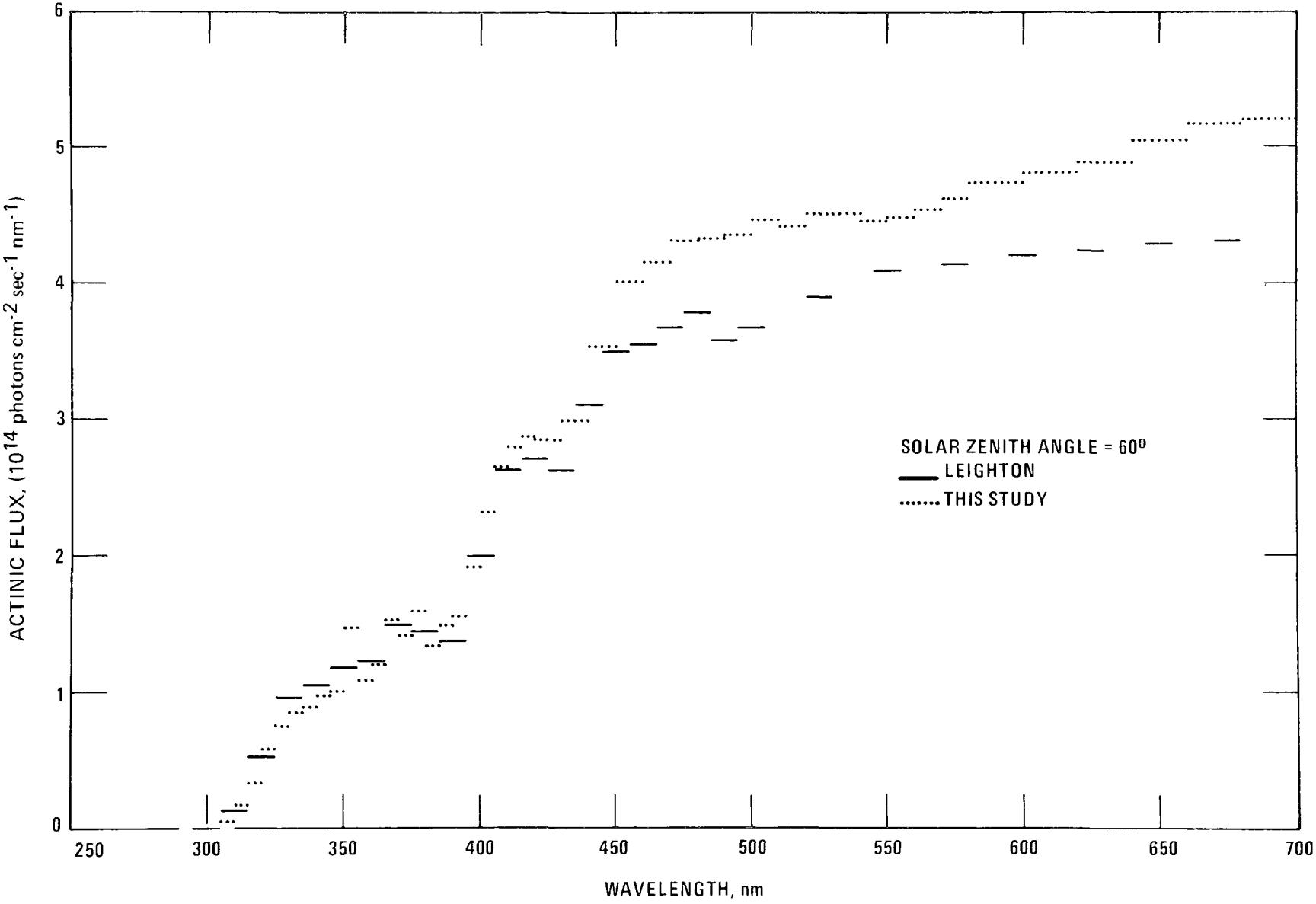

Figure 8. Calculated actinic flux (10^{14} photons cm^{-2} sec^{-1} nm^{-1}) averaged over indicated wavelength intervals (nm) at the earth's surface for solar zenith angle of 60° from this study (using best estimate albedos) and from Leighton.

representative cloud types, thicknesses, and densities.[3] Transmission functions developed from these data by Atwater and Brown (1974) are given in Table 12. They suggest that when clouds are present the clear sky fluxes should be multiplied by

$$\prod_{i=1}^{n} [1 - c_i(1 - T)] \qquad (5)$$

where n is the number of cloud layers present, c_i is the amount of cloud in each layer, and T represents the transmission of solar radiation through the specified cloud type (Table 12).

TABLE 12. TRANSMISSION (T) OF SOLAR RADIATION THROUGH VARIOUS CLOUD TYPES AS A FUNCTION OF OPTICAL AIR MASS (M) (FROM ATWATER AND BROWN, 1974).

CLOUD TYPE	EQUATION
Fog	T = 0.1626 + 0.0054 M
Stratus	T = 0.2684 - 0.0101 M
Stratocumulus	T = 0.3658 - 0.0149 M
Cumulus	T = 0.3658 - 0.0149 M
Cumulonimbus	T = 0.2363 + 0.0145 M
Altostratus	T = 0.4130 - 0.0014 M
Altocumulus	T = 0.5456 - 0.0236 M
Cirrus	T = 0.8717 - 0.0179 M
Cirrostratus	T = 0.9055 - 0.0638 M

The expression (5) and accompanying cloud transmissivities should only be considered as a rough approximation to the true effect of clouds on actinic flux. Variations of the vertical thickness of cloud layers are not taken into account. Moreover, Haurwitz' data are based on horizontal, not actinic, solar flux measurements. Our experience in making simultaneous

[3]Due to a typographical error, the transmissivity for cirrus at m = 2.0 should read 0.84 in Table 10 (page 40) of Leighton (1961).

measurements of the ultraviolet and all-wave solar flux has indicated that clouds do not attenuate the ultraviolet wavelengths as much as the longer wavelengths. Finally, these expressions should be used cautiously during partly cloudy conditions since the actual actinic flux may show large variability over short time periods as the sun is alternately behind and free of clouds.

A second approximate method for estimating the effect of clouds on actinic flux relies on continuous measurements of the incident radiation. A variety of commercial instruments are available for horizontal flux measurements. By comparing the measured flux to that expected for cloudless conditions, the amount of solar depletion resulting from a specific cloud situation can be estimated.

SECTION V

DISCUSSION

The data and computational techniques available to Leighton for his work on the application of solar radiation to photochemical pollution problems some 20 years ago have become outdated. Thus, this report was undertaken to redo, update, and expand upon his calculations of actinic flux. His results and those computed herein generally agree within 10% at wavelengths less than about 450 nm, which is a favorable reflection on this area of Leighton's work. However, this similarity in computed fluxes resulted partly because some of the errors in his data cancelled each other. For example, his extraterrestrial flux data were too high whereas his neglect of surface albedo led to reduced actinic fluxes. At wavelengths greater than 450 nm the two studies diverge significantly. The large albedo values used here at longer wavelengths caused the calculated actinic fluxes to be substantially greater than Leightons.

In this report the actinic fluxes calculated as a function of solar zenith angle and wavelength for "typical" atmospheric conditions are intended for general application. However, in some instances these data may be applied where the radiative characteristics of the atmospheric constituents are known to differ considerably from those used here. Therefore, a study of the dependence of the calculated fluxes on typical variations of the model input parameters was also undertaken. Various tabulations were presented here to give users information to adjust the actinic fluxes to their particular circumstance, when they have specific information on the input parameters. The actinic fluxes were generally shown to be relatively insensitive to changes of surface elevation and ozone concentrations,

and relatively sensitive to typical changes of atmospheric aerosols and surface albedo. The fluxes are directly dependent on the extraterrestrial solar flux.

An interesting aspect of these calculations was the description of the variation of actinic flux with height above the surface. Previously, only sketchy information was available on this topic, and most photochemical atmospheric diffusion models neglected to account for it. To show the importance of the vertical change of actinic flux, an estimate was made of the consequent change of the NO_2 photodissociation rate constant in the lowest kilometer of the atmosphere. The data indicated a rate constant increase of about 25% at small zenith angles to more than 50% at zenith angles of 70 and 78°.

REFERENCES

Atwater, M.A., and P.S. Brown, 1974: Numerical computations of the latitudinal variation of solar radiation for an atmosphere of varying opacity. J. Appl. Meteor., 13, 289-297.

Arvesen, J.C. et al., 1969: Determination of extraterrestrial solar spectral irradiance from a research aircraft. Appl. Optics, 11, 2215-2232.

Braslau, N., and J.V. Dave, 1973a: Effect of aerosols on the transfer of solar energy through realistic model atmospheres. Part I: Non-absorbing aerosols. J. Appl. Meteor., 12, 601-615.

Braslau, N., and J.V. Dave, 1973b: Effect of aerosols on the transfer of solar energy through realistic model atmospheres. Part II: Partly absorbing aerosols. J. Appl. Meteor., 12, 616-619.

Coulson, K.L., and D.W. Reynolds, 1971: The spectral reflectance of natural surfaces. J. Appl. Meteor., 10, 1285-1295.

Craig, R.A., 1965: The upper atmosphere. New York, Academic Press, 509 pp.

Dave, J.V., 1972: Development of programs for computing characteristics of ultraviolet radiation. Final Rept. under Contr. NAS 5-21680. NASA Rept. CR-139134. Nat. Aeronautics and Space Admin., Goddard Space Flight Ctr., Greenbelt, MD. (NTIS No. N75-10746/6SL). 27 pp.

DeLuisi, J.J., 1975: Measurements of the extraterrestrial solar radiant flux from 2981 to 4000 Å and its transmission through the earth's atmosphere as it is affected by dust and ozone. J. Geophys. Res., 80, 345-354.

Demerjian, K.L., et al., 1974: The mechanism of photochemical smog formation. In: Advances in Envr. Sci. and Technol., vol. 4, J. Pitts and R. Metcalf eds. New York, Wiley & Sons, p. 1-262.

Diermendjian, D., 1969: Electromagnetic scattering on spherical polydispersions. New York, Elsevier Publ. Co., 290 pp.

Dodge, M.C., and T.A. Hecht, 1975: Rate constant measurements needed to improve a general kinetic mechanism for photochemical smog. Int. J. Chem. Kinetics, 7, 155-163.

Edinger, J.G., 1973: Vertical distribution of photochemical smog in Los Angeles Basin. Environ. Sci. Technol., 7, 247-252.

Flowers, E.C., et al., 1969: Atmospheric turbidity over the United States, 1961-1966. J. Appl. Meteor., 8, 955-962.

Gloria, H.R. et al., 1974: Airborne survey of major air basins in California. J. Air Poll. Contr. Asso., 24, 645-652.

Haurwitz, B., 1948: Insolation in relation to cloud type. J. Meteor., 5, 110-113.

Herman, B.M., et al., 1971: The effect of atmospheric aerosols on scattered sunlight. J. Atm. Sci., 28, 419-428.

Howard, J.N. et al., 1960: Thermal radiation. Handbook of geophysics (Rev. Ed.). New York, McMillan, Chapt. 16.

Huschke, R.E., 1959: Glossary of meteorology. Boston, Amer. Meteorol. Soc., 638 pp.

Jackson, J.O. et al., 1975: Direct NO_2 photolysis rate monitor. Rev. Sci. Inst., 46, 376-378.

Komyhr, W.D. et al., 1973: Total ozone increase over North America during the 1960s. Pure and Appl. Geophys., 106-108, 981-999.

Labs, D. and H. Neckel, 1968: The radiation of the solar photosphere from 2000 Å to 100 μ. Zeitschrift fur Astrophysik, 69, 1-73.

Leighton, P.A., and W.A. Perkins, 1956: Solar radiation, absorption rates, and photochemical primary processes in urban air. Rept. No. 14, Air Poll. Found., Los Angeles, Calif. 129 pp.

Leighton, P.A., 1961: Photochemistry of air pollution. New York, Academic Press, 300 pp.

Lenschow, D.H., et al., 1964: Study of a continental surface albedo on the basis of flight measurements and structure of the earth's surface cover over North America. Mon. Wea. Rev., 92, 543-564.

Luther, F.M., and R.J. Gelinas, 1976: Effect of molecular multiple scattering and surface albedo on atmospheric photodissociation rates. J. Geophys. Res., 81, 1125-1132.

McClatchey, R.A. et al., 1972: Optical properties of the atmosphere (Third Ed.). Tech. Rept. AFCRL-72-0497, Air Force Cambridge Res. Labs., Bedford, Mass. 108 pp.

Nader, J.S., 1967: Pilot study of ultraviolet radiation in Los Angeles October 1965. Publ. No. 999-AP-38, Public Health Service, Nat. Ctr. for Air Poll. Control, Cincinnati, Ohio. 91 pp.

Penndorf, R., 1957: Tables of refractive index for standard air and the Rayleigh scattering coefficient for the spectral region between 0.2 and 20.0 μ and their application to atmospheric optics. J. Opt. Soc. Am., 47, 176-182.

Peterson, J.T., and E.C. Flowers, 1976: Interactions between air pollution and solar radiation. Int. Conf. on Environ. Sensing and Assessment, Las Vegas, Nev., Vol. 2, Paper 32-4, Inst. of Electrical & Electronics Eng., New York.

Peterson, J.T., and K.L. Demerjian, 1976: The sensitivity of computed ozone concentrations to ultraviolet radiation in the Los Angeles area. Atm. Environ. in press.

Rasool, S.I., and S.H. Schneider, 1971: Atmospheric carbon dioxide and aerosols: Effects of large increases on global climate. Science, 173, 138-141.

Reynolds, S.D., et al., 1973: Mathematical modeling of photochemical air pollution-I. Formulation of the model. Atm. Environ., 7, 1033-1061.

Sickles, J.E., and H.E. Jeffries, 1975: Development and operation of a device for the continuous measurement of ϕk_a for nitrogen dioxide. Publ. No. 396, Dept. of Environ. Sci. and Engin., Univ. No. Car., Chapel Hill, NC.

Thekaekara, M.P., 1974: Extraterrestrial solar spectrum, 3000-6100 Å at 1-Å intervals. Appl. Optics, 13, 518-522.

Yamamoto, G., and M. Tanaka, 1972: Increase of global albedo due to air pollution. J. Atm. Sci., 29, 1405-1412.

APPENDICES

APPENDIX A. VARIATION OF ATMOSPHERIC PRESSURE (mb), NUMBER OF ATMOSPHERIC AEROSOLS (cm^{-3}), AND OZONE CONCENTRATION ($g\ m^{-3}$) AS A FUNCTION OF HEIGHT ABOVE THE SURFACE (km) USED AS INPUT TO THE RADIATIVE TRANSFER MODEL.

HEIGHT (km)	PRESSURE (mb)	AEROSOLS (cm^{-3})	OZONE ($g\ m^{-3}$)
0	1.013E+03	8.62E+02	2.00E-04
1	9.020E+02	1.43E+02	2.00E-04
2	8.020E+02	1.77E+01	5.34E-05
3	7.100E+02	7.41E+00	5.54E-05
4	6.280E+02	2.45E+00	5.72E-05
5	5.540E+02	7.98E-01	5.89E-05
6	4.870E+02	6.21E-01	6.16E-05
7	4.260E+02	4.79E-01	6.70E-05
8	3.720E+02	3.69E-01	7.05E-05
9	3.240E+02	3.71E-01	7.68E-05
10	2.810E+02	3.73E-01	8.04E-05
11	2.430E+02	3.76E-01	9.82E-05
12	2.090E+02	4.19E-01	1.07E-04
13	1.790E+02	4.56E-01	1.34E-04
14	1.530E+02	5.07E-01	1.61E-04
15	1.300E+02	5.47E-01	1.70E-04
16	1.110E+02	5.87E-01	1.88E-04
17	9.500E+01	6.67E-01	2.14E-04
18	8.120E+01	7.35E-01	2.50E-04
19	6.950E+01	7.98E-01	2.86E-04
20	5.950E+01	8.84E-01	3.04E-04
21	5.100E+01	7.92E-01	3.21E-04
22	4.370E+01	6.78E-01	3.21E-04
23	3.760E+01	3.31E-01	3.04E-04
24	3.220E+01	1.54E-01	2.86E-04
25	2.770E+01	7.01E-02	2.68E-04
30	1.320E+01	2.68E-02	1.79E-04
35	6.520E+00	9.69E-03	8.22E-05
40	3.330E+00	3.53E-03	3.66E-05
45	1.760E+00	1.03E-03	1.16E-05
50	9.510E-01	2.85E-04	3.84E-06
55	4.850E-01	8.27E-05	1.43E-06
60	2.500E-01	2.34E-05	5.34E-07
65	1.300E-01	6.56E-06	2.01E-07
70	6.710E-02	1.88E-06	7.68E-08

APPENDIX B. VALUES OF MODEL INPUT DATA FOR EACH WAVELENGTH INTERVAL (nm): EXTRATERRESTRIAL SOLAR FLUX (ETR) IN W m^{-2} AND 10^{14} photons cm^{-2} sec^{-1}, OZONE ABSORPTION COEFFICIENT (O3ABS) IN cm atm^{-1}, NORMAL OZONE OPTICAL THICKNESS (O3OPT), NORMAL RAYLEIGH SCATTERING OPTICAL THICKNESS (R OPT), NORMAL AEROSOL SCATTERING OPTICAL THICKNESS (SCOPT), NORMAL AEROSOL EXTINCTION OPTICAL THICKNESS (EXOPT), AND SURFACE ALBEDO (ALB) IN %.

WAVELENGTH	ETR	ETR	O3ABS	O3OPT	R OPT	SCOPT	EXOPT	ALB
290-295	2.67	3.93	26.0	7.60	1.361	.203	.238	5.
295-300	2.75	4.11	14.0	4.09	1.265	.204	.238	5.
300-305	2.70	4.11	6.80	1.99	1.178	.205	.239	5.
305-310	3.17	4.91	3.50	1.02	1.098	.206	.240	5.
310-315	3.90	6.14	1.75	.511	1.025	.206	.240	5.
315-320	3.92	6.26	.90	.263	.958	.207	.241	5.
320-325	4.09	6.64	.48	.140	.896	.209	.242	5.
325-330	5.28	8.70	.25	.0730	.839	.210	.242	5.
330-335	5.19	8.69	.12	.0351	.788	.211	.243	5.
335-340	4.89	8.31	.055	.0161	.739	.211	.243	5.
340-345	5.09	8.78	.025	.0073	.694	.212	.244	5.
345-350	4.94	8.65	.010	.0029	.653	.213	.244	5.
350-355	5.47	9.70	.0045	.0013	.617	.214	.245	5.
355-360	4.92	8.86	.0020	.0006	.582	.215	.245	5.
360-365	5.34	9.74	-	-	.548	.216	.246	5.
365-370	6.43	11.91	-	-	.517	.217	.247	5.
370-375	5.70	10.69	-	-	.489	.217	.247	5.
375-380	6.24	11.85	-	-	.462	.218	.248	5.
380-385	5.07	9.77	-	-	.438	.219	.248	5.
385-390	5.48	10.69	-	-	.415	.219	.248	5.
390-395	5.55	10.96	-	-	.393	.220	.249	5.
395-400	6.62	13.25	-	-	.373	.221	.249	5.
400-405	7.68	15.57	-	-	.354	.221	.250	6.
405-410	8.49	17.41	-	-	.336	.222	.250	6.
410-415	8.81	18.30	-	-	.320	.222	.250	6.
415-420	8.80	18.15	-	-	.304	.223	.251	6.
420-430	16.93	36.23	-	-	.283	.224	.251	6.
430-440	16.94	37.10	-	-	.257	.225	.252	6.
440-450	19.15	42.91	.0031	.0009	.233	.226	.252	6.
450-460	20.47	46.89	.0045	.0013	.213	.227	.252	8.
460-470	20.49	47.97	.0080	.0023	.195	.227	.252	8.
470-480	20.49	49.00	.0105	.0031	.178	.228	.253	8.
480-490	19.94	48.70	.019	.0054	.163	.229	.253	8.
490-500	19.54	48.69	.022	.0063	.151	.229	.253	8.
500-510	19.16	48.72	.038	.0110	.139	.230	.254	10.
510-520	18.45	47.85	.041	.0118	.128	.230	.254	10.
520-530	18.45	48.76	.054	.0158	.119	.231	.254	10.
530-540	18.15	48.90	.069	.0202	.110	.231	.254	10.
540-550	17.54	48.13	.078	.0228	.102	.231	.254	10.
550-560	17.15	47.93	.089	.0260	.0946	.231	.254	11.

APPENDIX B. CONTINUED

WAVELENGTH	ETR	ETR	O3ABS	O3OPT	R OPT	SCOPT	EXOPT	ALB
560-570	17.04	48.48	.103	.0301	.0880	.232	.253	11.
570-580	17.16	49.69	.118	.0345	.0819	.232	.253	11.
580-600	33.92	100.78	.113	.0330	.0737	.232	.253	11.
600-620	32.67	100.36	.117	.0342	.0643	.231	.252	12.
620-640	31.43	99.70	.091	.0266	.0564	.231	.251	12.
640-660	30.26	99.04	.063	.0184	.0497	.230	.250	13.5
660-680	29.13	98.26	.042	.0123	.0440	.229	.248	15.
680-700	28.00	97.28	.027	.0079	.0391	.228	.247	15.

APPENDIX C. TABULATION OF SOLAR ZENITH ANGLES AS A FUNCTION OF TRUE SOLAR TIME AND MONTH. FOR DETERMINATION OF AFTERNOON VALUES, THE TABLE IS SYMMETRIC ABOUT NOON. FOUR TABLES ARE PRESENTED FOR LATITUDES 20, 30, 40, AND 50°N.

TRUE SOLAR TIME

	0400	0430	0500	0530	0600	0630	0700	0730	0800	0830	0900	0930	1000	1030	1100	1130	1200
Latitude 20°N																	
JANUARY 1							84.9	78.7	72.7	66.1	61.5	56.5	52.1	48.3	45.5	43.6	43.0
FEBRUARY 1						88.9	82.5	75.8	69.6	63.3	57.7	52.2	47.4	43.1	40.0	37.8	37.2
MARCH 1						85.7	78.8	72.0	65.2	58.6	52.3	46.2	40.5	35.5	31.4	28.6	27.7
APRIL 1					88.5	81.5	74.4	67.4	60.3	53.4	46.5	39.7	33.2	26.9	21.3	17.2	15.5
MAY 1					85.0	78.2	71.2	64.3	57.2	50.2	43.2	36.1	29.1	26.1	15.2	8.8	5.0
JUNE 1				89.2	82.7	76.0	69.3	62.5	55.7	48.8	41.9	35.0	28.1	21.1	14.2	7.3	2.0
JULY 1				88.8	82.3	75.7	69.1	62.3	55.5	48.7	41.8	35.0	28.1	21.2	14.3	7.7	3.1
AUGUST 1					83.8	77.1	70.2	63.3	56.4	49.4	42.4	35.4	28.3	21.3	14.3	7.3	1.9
SEPTEMBER 1					87.2	80.2	73.2	66.1	59.1	52.1	45.1	38.1	31.3	24.7	18.6	13.7	11.6
OCTOBER 1						84.1	77.1	70.2	63.3	56.5	49.9	43.5	37.5	32.0	27.4	24.3	23.1
NOVEMBER 1						87.8	81.3	74.5	68.3	61.8	56.0	50.2	45.3	40.7	37.4	35.1	34.4
DECEMBER 1							84.3	78.0	71.8	66.1	60.5	55.6	50.9	47.2	44.2	42.4	41.8
Latitude 30°N																	
JANUARY 1							89.4	83.7	78.3	73.2	68.4	64.1	60.4	57.3	55.0	53.5	53.0
FEBRUARY 1							86.2	80.3	74.6	69.1	64.1	59.4	55.3	51.9	49.3	47.7	47.2
MARCH 1						87.5	81.1	74.9	68.8	62.9	57.4	52.2	47.5	43.5	40.3	38.4	37.7
APRIL 1					87.2	81.4	74.9	68.5	62.1	55.8	49.6	43.8	38.2	33.3	29.3	26.5	25.5
MAY 1				88.9	82.7	76.3	69.9	63.4	56.9	50.4	44.0	37.6	31.4	25.6	20.4	16.5	15.0
JUNE 1				85.3	79.2	73.1	66.8	60.4	54.0	47.5	41.0	34.5	28.1	21.7	15.7	10.5	8.0
JULY 1				84.7	78.7	72.5	66.3	60.0	53.5	47.1	40.6	34.1	27.7	21.2	15.1	9.6	6.9
AUGUST 1				87.2	81.0	74.7	68.3	61.9	55.4	48.9	42.4	36.0	29.7	23.6	18.1	13.7	11.9
SEPTEMBER 1					85.9	79.4	72.9	66.4	60.0	53.6	47.3	41.2	35.5	30.2	25.8	22.8	21.6
OCTOBER 1						85.1	78.7	72.4	66.2	60.1	54.4	48.8	43.8	39.5	36.1	33.9	33.1
NOVEMBER 1							84.6	78.4	72.8	67.1	62.0	57.0	53.0	49.3	46.7	44.9	44.4
DECEMBER 1							88.7	82.8	77.3	72.2	67.3	63.0	59.2	56.0	53.7	52.2	51.8

APPENDIX C. CONTINUED

	TRUE SOLAR TIME																
	0400	0430	0500	0530	0600	0630	0700	0730	0800	0830	0900	0930	1000	1030	1100	1130	1200
Latitude 40°																	
JANUARY 1								89.0	84.2	79.8	75.7	72.1	69.0	66.4	64.6	63.4	63.0
FEBRUARY 1								84.8	79.8	75.2	70.7	67.0	63.5	60.9	58.8	57.6	57.2
MARCH 1						89.1	83.7	78.1	72.8	67.8	63.1	58.8	55.1	51.9	49.6	48.1	47.7
APRIL 1					87.1	81.4	75.6	70.0	64.4	59.0	53.8	49.0	44.6	40.9	38.0	36.2	35.5
MAY 1				85.9	80.5	74.7	68.9	63.2	57.5	51.8	46.3	41.0	36.1	31.7	28.2	25.8	25.0
JUNE 1			86.8	81.5	76.1	70.5	64.9	59.2	53.4	47.7	42.0	36.5	31.2	26.2	22.1	19.1	18.0
JULY 1			86.0	80.8	75.4	69.9	64.3	58.6	52.8	47.1	41.4	35.8	30.4	25.4	21.1	18.0	16.9
AUGUST 1			89.3	83.9	78.4	72.8	67.1	61.4	55.6	49.9	44.4	39.0	33.8	29.2	25.4	22.8	21.9
SEPTEMBER 1					84.6	78.9	73.2	67.5	61.8	56.3	51.0	46.0	41.4	37.5	34.4	32.3	31.6
OCTOBER 1						86.3	80.6	75.1	69.7	64.5	59.6	55.1	51.2	47.8	45.3	43.6	43.1
NOVEMBER 1							88.1	82.6	77.8	72.8	68.6	64.4	61.1	58.2	56.1	54.7	54.4
DECEMBER 1								88.1	83.3	78.8	74.7	71.0	67.8	65.3	63.3	62.2	61.8
Latitude 50°																	
JANUARY 1										86.5	83.2	80.2	77.7	75.7	74.2	73.3	73.0
FEBRUARY 1								89.5	85.3	81.5	78.0	74.9	72.2	70.0	68.5	67.5	67.2
MARCH 1							86.3	81.8	77.4	73.3	69.6	66.2	63.2	60.9	59.1	58.0	57.7
APRIL 1					86.6	81.8	76.9	72.2	67.6	63.2	59.1	55.4	52.0	49.3	47.2	45.9	45.5
MAY 1			87.8	83.2	78.5	73.7	68.9	64.1	59.4	54.7	50.3	46.2	42.5	39.4	37.0	35.5	35.0
JUNE 1		86.7	82.4	78.0	73.3	68.6	63.8	59.0	54.2	49.5	44.9	40.6	36.6	33.1	30.4	28.6	28.0
JULY 1	89.7	85.7	81.5	77.1	72.5	67.8	63.0	58.2	53.4	48.7	44.1	39.7	35.6	32.1	29.3	27.5	26.9
AUGUST 1		89.7	85.4	80.8	76.2	71.4	66.6	61.8	57.0	52.4	47.9	43.7	39.9	36.6	34.1	32.5	31.9
SEPTEMBER 1				88.3	83.6	78.8	74.0	69.2	64.6	60.1	55.9	52.0	48.5	45.7	43.5	42.1	41.6
OCTOBER 1						87.6	82.8	78.2	73.8	69.6	65.7	62.1	59.1	56.5	54.7	53.5	53.1
NOVEMBER 1								87.1	83.0	79.0	75.5	86.2	69.5	67.3	65.7	64.7	64.4
DECEMBER 1									89.2	85.5	82.1	79.1	76.5	74.5	73.0	72.1	71.8

TECHNICAL REPORT DATA
(Please read Instructions on the reverse before completing)

1. REPORT NO.	2.	3. RECIPIENT'S ACCESSION NO.
EPA-600/4-76-025		

4. TITLE AND SUBTITLE	5. REPORT DATE
CALCULATED ACTINIC FLUXES (290 - 700 nm) FOR AIR POLLUTION PHOTOCHEMISTRY APPLICATIONS	June 1976
	6. PERFORMING ORGANIZATION CODE

7. AUTHOR(S)	8. PERFORMING ORGANIZATION REPORT NO.
James T. Peterson	

9. PERFORMING ORGANIZATION NAME AND ADDRESS	10. PROGRAM ELEMENT NO.
Environmental Sciences Research Laboratory Office of Research and Development U. S. Environmental Protection Agency Research Triangle Park, NC 27711	1AA009
	11. CONTRACT/GRANT NO.

12. SPONSORING AGENCY NAME AND ADDRESS	13. TYPE OF REPORT AND PERIOD COVERED
Environmental Sciences Research Laboratory Office of Research and Development U. S. Environmental Protection Agency Research Triangle Park, NC 27711	In-House
	14. SPONSORING AGENCY CODE EPA - ORD

15. SUPPLEMENTARY NOTES

16. ABSTRACT

Calculations are presented of the actinic (spherically integrated) solar flux from 290 to 700 nm at solar zenith angles between 0 and 86°. The calculated values are obtained by using a radiative transfer program (developed by Dave) that accounts for molecular scattering, ozone absorption, and aerosol scattering and absorption. Input data consists of aerosol size distribution, aerosol number and ozone concentrations as a function of height, aerosol index of refraction, and the following as a function of wavelength: ozone absorption coefficient, molecular scattering coefficient, solar constant, and surface reflectivity. The calculated actinic flux values are evaluated for their dependence on variations of surface reflectivity, aerosol amount, ozone amount and station elevation. The variation of the actinic flux with altitude above the surface is discussed with emphasis on the change through the lowest kilometer of the atmosphere. Finally, the flux values presented here are compared to those of Leighton (1961); the differences in the methodology and input data between the two studies are illustrated. These calculated actinic flux data are useful for estimating photodissociation rate constants for application to photochemical air pollution problems.

17. KEY WORDS AND DOCUMENT ANALYSIS

a. DESCRIPTORS	b. IDENTIFIERS/OPEN ENDED TERMS	c. COSATI Field/Group
*Air pollution		13B
*Solar radiation		03B
Radiant flux density		20F
Computation		12A
*Aerosols		07D
*Photochemical reactions		17E
*Reaction kinetics		14B
*Atmospheric models		

18. DISTRIBUTION STATEMENT	19. SECURITY CLASS *(This Report)*	21. NO. OF PAGES
RELEASE TO PUBLIC	UNCLASSIFIED	63
	20. SECURITY CLASS *(This page)*	22. PRICE
	UNCLASSIFIED	

EPA Form 2220-1 (9-73)